# α-Synuclein and ALPS motifs are membrane curvature sensors whose contrasting chemistry mediates selective vesicle binding

Iwona M. Pranke,[1] Vincent Morello,[2] Joëlle Bigay,[2] Kimberley Gibson,[4] Jean-Marc Verbavatz,[3,4] Bruno Antonny,[2] and Catherine L. Jackson[1]

[1]Laboratoire d'Enzymologie et Biochimie Structurales, Centre de Recherche de Gif, Centre National de la Recherche Scientifique 91198 Gif-sur-Yvette, France
[2]Institut de Pharmacologie Moléculaire et Cellulaire, Centre National de la Recherche Scientifique et Université de Nice Sophia Antipolis, 06560 Valbonne, France
[3]Institut de biologie et de technologies de Saclay, Commissariat à l'Energie Atomique, Saclay F-91191, France
[4]Max Planck Institute of Molecular Cell Biology and Genetics, 01307 Dresden, Germany

Membrane curvature sensors have diverse structures and chemistries, suggesting that they might have the intrinsic capacity to discriminate between different types of vesicles in cells. In this paper, we compare the in vitro and in vivo membrane-binding properties of two curvature sensors that form very different amphipathic helices: the amphipathic lipid-packing sensor (ALPS) motif of a Golgi vesicle tether and the synaptic vesicle protein α-synuclein, a causative agent of Parkinson's disease. We demonstrate the mechanism by which α-synuclein senses membrane curvature. Unlike ALPS motifs, α-synuclein has a poorly developed hydrophobic face, and this feature explains its dual sensitivity to negatively charged lipids and to membrane curvature. When expressed in yeast cells, these two curvature sensors were targeted to different classes of vesicles, those of the early secretory pathway for ALPS motifs and to negatively charged endocytic/post-Golgi vesicles in the case of α-synuclein. Through structures with complementary chemistries, α-synuclein and ALPS motifs target distinct vesicles in cells by direct interaction with different lipid environments.

## Introduction

COP (coat protein)-mediated trafficking in the early secretory pathway and clathrin-mediated endocytosis are similar processes that involve dynamic cycles of vesicle budding and fusion. Each starts with assembly of a coat on a membrane (COPII, COPI, or clathrin), deformation of the membrane into a bud, and then fission to release the transport vesicle (Bonifacino and Glick, 2004). Targeting of the vesicle and uncoating precede vesicle fusion, which is mediated by SNARE proteins (Jahn and Scheller, 2006; Wickner and Schekman, 2008; Südhof and Rothman, 2009). These processes involve significant changes in the curvature of the membrane, and proteins that bind specifically to highly curved membranes, including amphipathic lipid-packing sensor (ALPS) motifs and BAR domains, play important roles in regulation of vesicle budding fusion cycles (McMahon and Gallop, 2005; Frost et al., 2009; Drin and Antonny, 2010). The ALPS motif was originally identified in ArfGAP1, which hydrolyzes GTP on Arf1 in COPI vesicles, thus coupling release of the coat with completion of vesicle formation (Bigay et al., 2005; Mesmin et al., 2007). An ALPS motif is also found at the N terminus of the long coiled-coil (CC) tether GMAP-210, which is involved in trafficking within the early secretory pathway (Cardenas et al., 2009). The tethering reaction of GMAP-210 has been reconstituted in vitro, showing that the N-terminal ALPS motif binds to small vesicles, whereas the C terminus binds to flatter membranes (Drin et al., 2008).

Several ALPS motifs are present in proteins that function in the early secretory pathway and the nuclear envelope (Drin et al., 2007; Doucet et al., 2010). These membranes are characterized

Correspondence to Catherine L. Jackson: jackson@ijm.univ-paris-diderot.fr; or Bruno Antonny: antonny@ipmc.cnrs.fr

I.M. Pranke's and C.L. Jackson's present address is Institut Jacques Monod, Centre National de la Recherche Scientifique et Université Paris Diderot, 75205 Paris, France.

Abbreviations used in this paper: AH, amphipathic helix; ALPS, amphipathic lipid-packing sensor; CC, coiled coil; CPY, carboxypeptidase Y; DMF, dimethyl formamide; mRFP, monomeric RFP; PC, phosphatidylcholine; PE, phosphatidylethanolamine; PM, plasma membrane; PO, palmitoyl oleoyl; PS, phosphatidylserine; yEGFP, yeast EGFP.



Supplemental material can be found at:
http://doi.org/10.1083/jcb.201011118

The Rockefeller University Press $30.00
J. Cell Biol. Vol. 194 No. 1 89–103
www.jcb.org/cgi/doi/10.1083/jcb.201011118

by a low surface charge, low levels of cholesterol, and phospholipids with largely monounsaturated fatty acid side chains (van Meer et al., 2008). Another major lipid environment in the endomembrane system of eukaryotic cells, found in early endosomes, the TGN, and the plasma membrane (PM), has different physical properties. These membranes are rich in cholesterol, their phospholipids have predominantly saturated fatty acids, and they exhibit asymmetry, with the cytosolic leaflet enriched in phosphatidylserine (PS) and other anionic phospholipids (van Meer et al., 2008). The distinct lipid compositions of the ER–early Golgi and TGN–endosomal–PM membrane systems have been conserved in evolution (Schneiter et al., 1999), and recent data on the properties of transmembrane proteins suggest these two lipid environments are maintained as distinct entities, with a sharp transition occurring within the Golgi apparatus (Sharpe et al., 2010).

ALPS motifs bind specifically to highly curved membranes because they are unbalanced lipid-binding amphipathic helices (AHs), having a well-developed hydrophobic face but very few charged residues on their polar face (Drin et al., 2007). Unlike a typical AH, which uses both hydrophobic and electrostatic interactions to associate with membranes, the lack of charged residues on the polar face of an ALPS AH makes it solely dependent on the hydrophobic force for membrane association. Hence, an ALPS motif is unable to associate with a flat bilayer of physiological composition, and requires lipid-packing defects, such as those created upon bending the membranes of the early secretory pathway.

A protein that forms a very different type of AH has also been reported to bind preferentially to highly curved membranes (Davidson et al., 1998; Middleton and Rhoades, 2010). This protein, α-synuclein, plays a central role in Parkinson's disease, a debilitating neurodegenerative disorder (Auluck et al., 2010). The precise function of α-synuclein in cells is not known, but it is expressed primarily in neurons, in which it localizes to synaptic vesicles (Kahle et al., 2000). α-Synuclein is involved in maintaining the reserve pool of synaptic vesicles before release and may act as a regulator of synaptic vesicle fusion (Larsen et al., 2006; Burré et al., 2010). Like ALPS motifs, α-synuclein is unfolded in solution but forms an AH upon contact with the appropriate membrane (Davidson et al., 1998). Spin labeling experiments have determined that α-synuclein forms a long 3–11 helix upon binding to membranes, with a highly regular repeated structure that features lysine residues at the interface between the polar and hydrophobic faces (Jao et al., 2008). In contrast to an ALPS motif, the hydrophobic face of α-synuclein is restrained, consisting of small hydrophobic residues, such as valine, alanine, and even threonine. How this type of AH acts as a curvature sensor is not clear.

We report here the mechanism by which α-synuclein senses membrane curvature in vitro and compare it with that used by an ALPS motif. For in vivo experiments, we chose the yeast system because neither α-synuclein nor the GMAP-210 ALPS motif has a yeast homologue, thus minimizing the occurrence of protein–protein interactions that could complicate analysis of their lipid-binding properties. In yeast cells, the GMAP-210 ALPS motif and α-synuclein are targeted to different types of vesicles. Our results support the conclusion that the AHs of ALPS motifs and α-synuclein can discriminate different vesicles in cells through direct interaction with a lipid environment complementary to each one's distinctive chemistry.

## Results

### The GMAP-210 ALPS motif and α-synuclein both cause accumulations of vesicles in cells

We expressed the N-terminal region of GMAP-210 ($GMAP_N$) and full-length α-synuclein as GFP or mCherry fusions in yeast cells (Fig. 1). $GMAP_N$-mCherry and $GMAP_N$-GFP localized to cytoplasmic puncta (Figs. 1 A and S1 A), which EM revealed to be clusters of small vesicles (Fig. 1 B). α-Synuclein–GFP also localized to cytoplasmic structures composed of vesicles (Fig. 1, C and D), as has been reported previously (Gitler et al., 2008; Soper et al., 2008). The $GMAP_N$ structures were made up of a regular arrangement of vesicles ∼50 nm in diameter, which by immuno-EM analysis were shown to contain the $GMAP_N$-GFP protein (Figs. 1 E and S1 B). We determined the concentration of $GMAP_N$-GFP in yeast cells to be ∼7 µM (Fig. S1 C), giving a protein/phospholipid ratio of ∼1:1,000 (see Materials and methods). Based on in vitro experiments (Drin et al., 2008), this ratio is consistent with $GMAP_N$ binding to vesicles after their formation, rather than inducing them. Expression of either $GMAP_N$ or α-synuclein led to a severe defect in cell growth (Fig. 1 F) and a significant slowing of ER to Golgi transport (Fig. S1 D). For α-synuclein, our results are consistent with a previous study (Outeiro and Lindquist, 2003).

$GMAP_N$ and α-synuclein vesicular structures differed in their position with respect to the cell periphery. $GMAP_N$ structures were randomly distributed throughout the cell (Figs. 1 A and S1 A): only 10% were located in close proximity to the cell periphery (Fig. S1 E). In contrast, ∼80% of α-synuclein structures were tightly juxtaposed to the PM (Figs. 1 C and S1 E). When $GMAP_N$-mCherry and α-synuclein–GFP were coexpressed together, distinct structures were observed, and they did not colocalize at early time points after induction (Fig. 1 G). These results indicate that expression of $GMAP_N$ and α-synuclein in yeast cells leads to accumulation of clusters of small vesicles and is consistent with the idea that they bind to and trap vesicles in cells. However, they also suggest that the vesicles trapped by these two proteins are different.

### Comparison of the ALPS motif and α-synuclein lipid-binding properties in vitro

Examination of the amphipathic structures formed by $GMAP_N$ and α-synuclein reveals striking differences (Fig. 2, A and B). The N-terminal region of α-synuclein forms an amphipathic 3–11 helix, with properties opposite to the amphipathic α-helix formed by an ALPS motif, both in terms of electrostatics and hydrophobicity. The contrasting chemistries of $GMAP_N$ and α-synuclein AHs suggest that they might be adapted to membranes of different lipid composition, providing a straightforward explanation for their localization to different vesicular

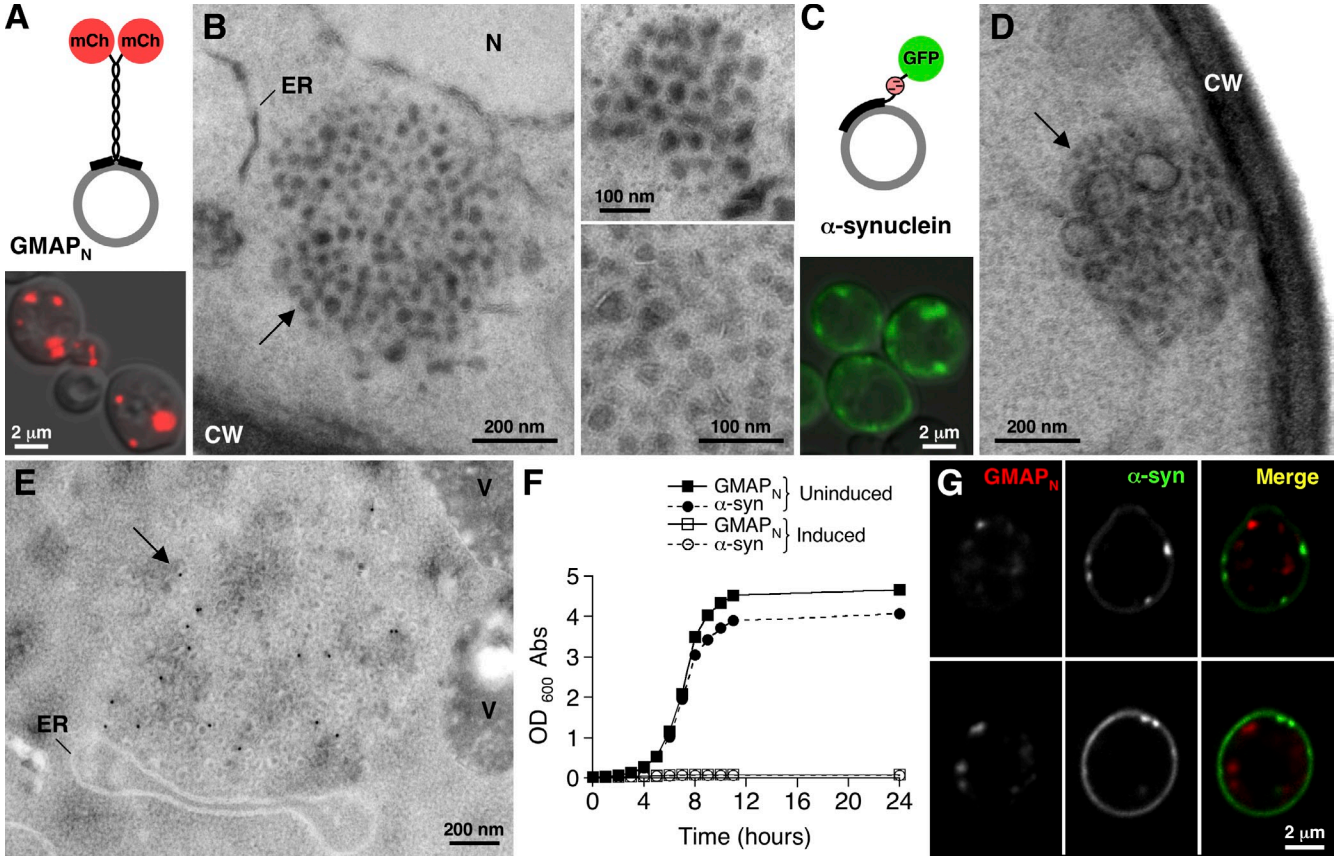


Figure 1. **GMAP$_N$ and α-synuclein cause accumulations of distinct vesicular structures in yeast cells.** (A, top) Schematic diagram of GMAP$_N$-mCherry (mCh). (bottom) Localization of this construct in yeast cells. (B) Representative transmission EM images of cells expressing GMAP$_N$-GFP. (C, top) Schematic diagram of α-synuclein–GFP. (bottom) Localization in yeast cells. (D) Representative EM image of cells expressing α-synuclein–GFP. (E) Immunogold labeling of cells expressing GMAP$_N$-GFP using antibodies against GFP. Arrows show vesicular structures. N, nucleus; V, vacuole; ER, endoplasmic reticulum; CW, cell wall. (F) Strains IPY4 GMAP$_N$-GFP and IPY5 α-synuclein (α-syn)–GFP were grown overnight under repressing conditions and then shifted (open symbols) or not shifted (closed symbols) to induction medium for the indicated times, and absorbance (Abs) of the cultures at OD$_{600}$ was monitored. (G) Localization of GMAP$_N$-mCherry and α-synuclein–GFP expressed together in wild-type yeast cells. (top and bottom) Two optical sections of a z stack obtained for a single cell. BY4742 cells carrying the indicated proteins on plasmids were grown overnight (A–E) or for 4 h (G) under inducing conditions and imaged.

structures in yeast cells (Fig. 1). Nevertheless, what remains disconcerting is the fact that if both ALPS motifs and α-synuclein recognize membrane curvature, two very different chemistries can lead to the same function.

To compare the lipid-binding properties of GMAP$_N$ and α-synuclein in vitro, we used constructs similar to those expressed in yeast except that they were not fused to a fluorescent protein but were covalently labeled with a lipid-sensitive fluorescent probe (NBD; Johnson, 2005) through a cysteine introduced at the beginning of the AH (Fig. 2, A and B). Experiments were conducted by incubating the NBD-labeled constructs with liposomes of defined size and composition and by immediately recording the fluorescence emission spectrum of the mixture. A low protein/lipid ratio (1:600 to 1:1,200) was used to minimize surface-crowding effects. Titration experiments showed that the fluorescence of NBD increased 4.5-fold for GMAP$_N$ and 10-fold for α-synuclein upon liposome binding (see next two paragraphs). Note that GMAP$_N$ is a dimer. Hence, it uses two ALPS motifs to bind to lipid membranes, which corresponds to 38 × 2 = 76 aa (Fig. 2 A), a number comparable with the continuous 90 aa AH of α-synuclein (Fig. 2 B).

Fig. 2 (C and D) compares the fluorescence emission spectra of GMAP$_N$ and α-synuclein with or without size-calibrated liposomes made exclusively of neutral lipids (egg phosphatidylcholine [PC]/palmitoyl oleoyl phosphatidylethanolamine [POPE] = 7:3; cholesterol/phospholipids = 1:5). Although GMAP$_N$ bound to these liposomes in a sharply curvature-dependent manner (Fig. 2 C, partition coefficients in bottom inset), α-synuclein was unable to bind to these liposomes, except for weak binding to the smallest ones (radius = 31 nm; Fig. 2 D). Similar results were obtained with liposomes of a composition similar to that of Golgi membranes ("Golgi mix"), which contain a relatively low fraction of anionic lipids (5 mole percent [mol%] PS and 10 mol% phosphatidylinositol; Fig. S2 A). These results indicate that the ALPS motif, but not α-synuclein, is adapted to curved membranes containing low amounts of anionic lipids and even to neutral liposomes.

PS is the major anionic lipid of eukaryotic cellular membranes and is known to favor the binding of α-synuclein (Davidson et al., 1998). As observed previously for other ALPS motifs, we observed no major change in the binding properties of GMAP$_N$ by the introduction of POPS (Fig. S2 B). In striking contrast, the introduction of increasing amounts of POPS at the expense of

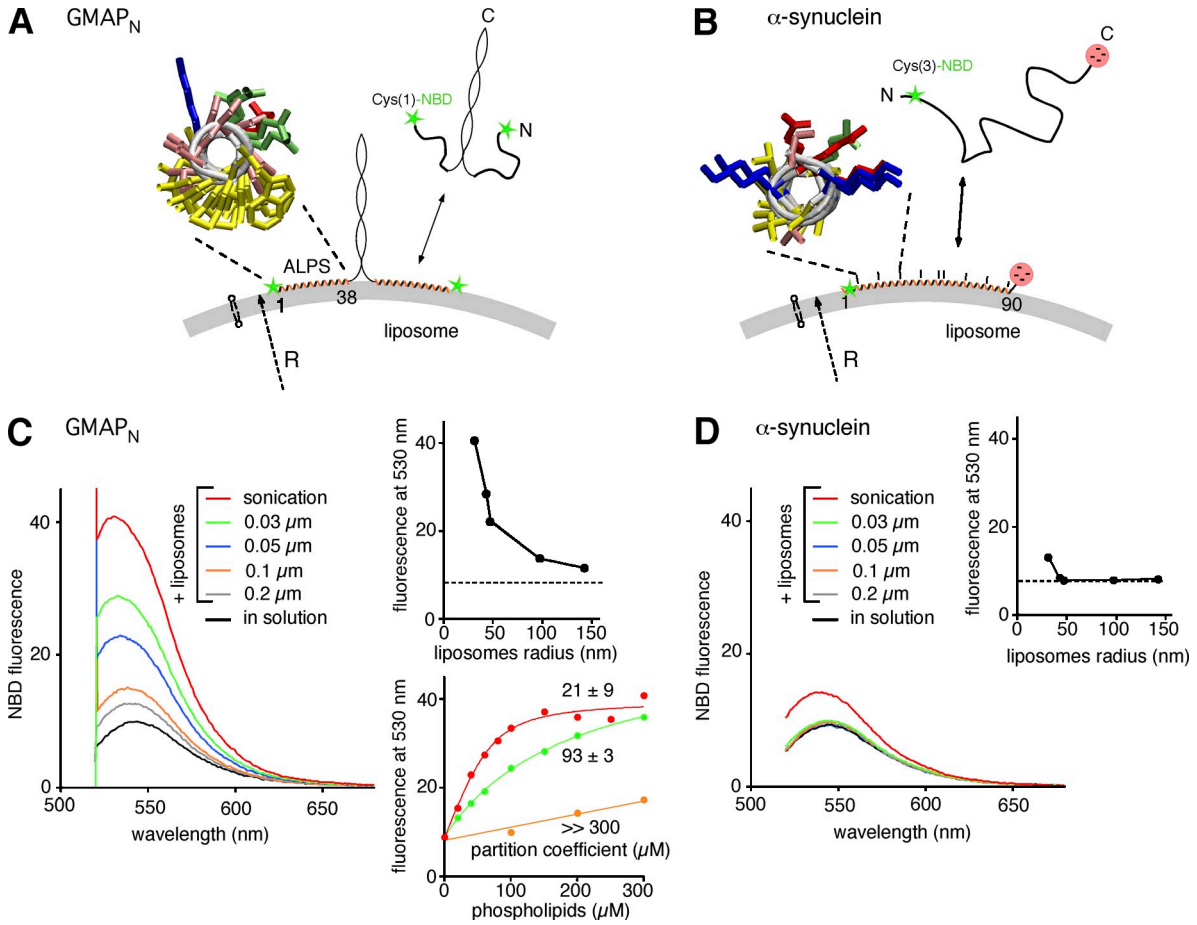


Figure 2. **GMAP$_N$, but not α-synuclein, is a sensor of the curvature of neutral lipid membranes.** (A and B) Structural features of the ALPS motif of GMAP-210 (aa 1–38) and of the α-synuclein AH and principles of the liposome-binding experiments. (A) The ALPS motif of GMAP-210 is assumed to form a perfect α helix. The structure of α-synuclein is from recent electron paramagnetic resonance experiments (Jao et al., 2008). (B) For clarity, only two 11-mer repeats (aa 9–30) are shown, but the remainder of the AH displays the same features. Yellow: Ala, Val, Leu, Ile, Met, Phe, and Trp. Pink: Ser, Thr, and Gly. Red: Asp and Glu. Blue: Lys and Arg. Green: other residues. To monitor lipid binding, the constructs were labeled with NBD on a cysteine at the beginning of the AH (mutations M1C in GMAP$_N$ and V3C in α-synuclein). The drawing is approximately to scale for a liposome of radius (R) = 30 nm. (C and D) Emission fluorescence spectra of [NBD]GMAP$_N$ (C) or [NBD]α-synuclein (D; 125 nM each) with or without calibrated neutral liposomes obtained by extrusion through polycarbonate filters of defined pore size or sonication (150 μM phospholipids; egg PC/POPE = 7:3; cholesterol/phospholipids = 1:5). (top insets) Fluorescence level at 530 nm as a function of liposome radius (as determined by dynamic light scattering). The horizontal lines indicate the fluorescence level in the absence of liposomes. (C, bottom inset) Fluorescence at 530 nm of 125 nM [NBD]GMAP$_N$ as a function of phospholipid concentration. Color coding for sonicated and extruded liposomes is indicated on the left. Calculation of partition coefficients is as previously described (see Materials and methods; Mesmin et al., 2007). N, N terminus; C, C terminus.

POPC in small liposomes dramatically increased the binding of α-synuclein (Fig. 3 A). Conversely, when liposomes of varying radii and containing a constant amount of POPS (60 or 30 mol%) were used, we observed that α-synuclein bound to liposomes in a sharply size-dependent manner (Figs. 3 B, partition coefficients in inset; and S2 C). The binding of α-synuclein was so sensitive to both PS and membrane curvature that the amount of PS required for binding decreased dramatically when the liposome radius changed only a small amount, from a mean of 48 to 30 nm (Fig. 3 A, right). These direct in vitro comparisons of ALPS motifs and α-synuclein demonstrate that they have similar responses to membrane curvature but different lipid requirements for binding.

### Mechanism by which α-synuclein senses membrane curvature

ALPS motifs are defined by the abundance of small and uncharged residues (Ser, Thr, and Gly) on their polar face and by the paucity of charged residues (Fig. 2 A). These features are responsible for the high sensitivity of ALPS motifs to membrane curvature because introducing positively charged residues at the two edges of the polar face strongly reduces their curvature sensitivity (Drin et al., 2007). α-Synuclein represents a striking counterexample to this rule, as its polar face displays an almost perfect distribution of positively charged residues at its two edges (Fig. 2 B). This poses the question of how α-synuclein senses membrane curvature.

Although opposite in chemistry, α-synuclein and the ALPS motif share the property of being unbalanced AHs, with either the charged or hydrophobic face being much less developed than that of classical AHs. We hypothesized that α-synuclein is a curvature sensor because of its poor hydrophobic face and sought to test this model by enhancing the hydrophobicity of this face. We chose to mutate the six threonine residues that are regularly spaced along the α-synuclein helix and that, when

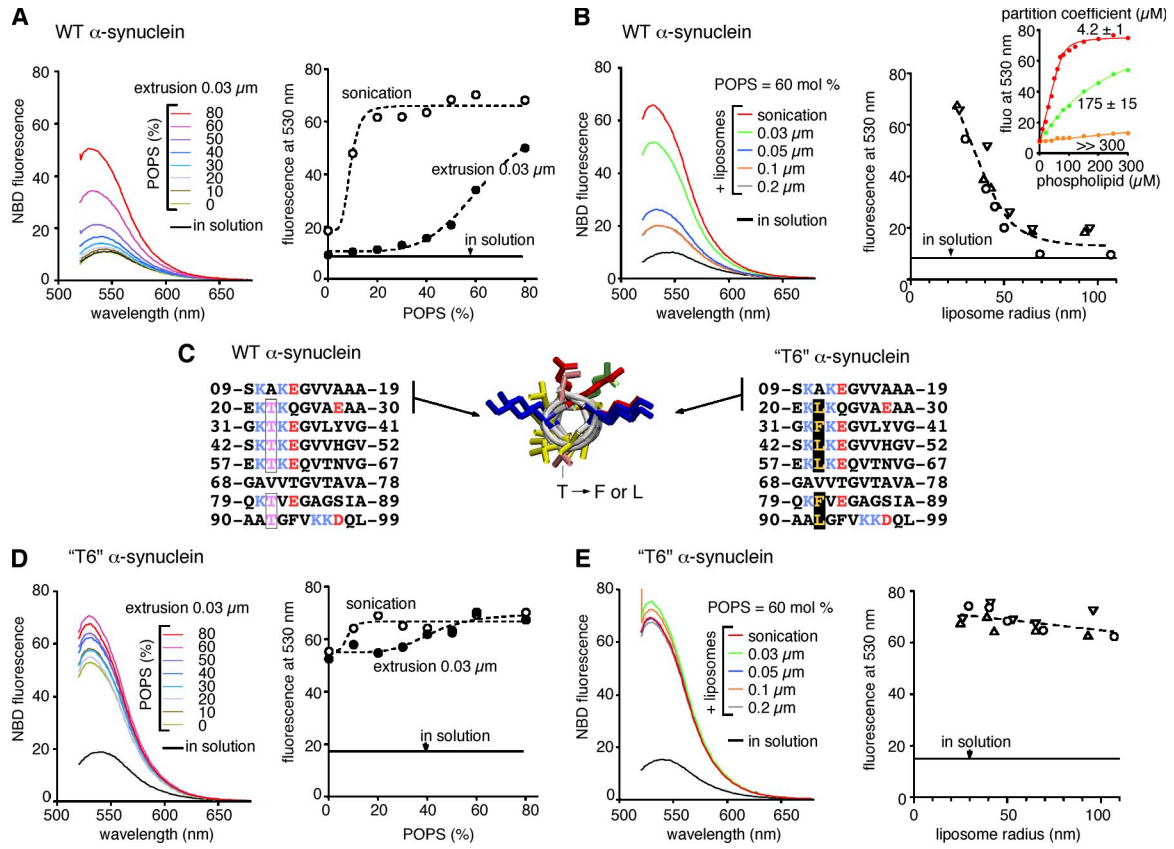


Figure 3. **The ability of α-synuclein to sense the curvature of negatively charged lipid membranes depends on its poorly developed hydrophobic face.** (A) Binding of wild-type α-synuclein to small liposomes containing increasing amounts of POPS (0–80 mol%) at the expense of POPC (80–0 mol%). The remaining phospholipid was egg PC (20 mol%) and the cholesterol/phospholipid ratio was 1:2. The liposomes were obtained by extrusion through 30-nm polycarbonate filters. The plot reports the fluorescence at 530 nm as determined from the spectra shown on the left as well as from an experiment performed with sonicated liposomes of the same composition. The extruded and sonicated liposomes displayed radii in the range of 46–53 and 23–48 nm, respectively. (B) Binding of wild-type α-synuclein to size-calibrated charged liposomes (egg PC/POPS = 4:6; cholesterol/phospholipids = 1:2). The three symbols used in the right plot correspond to three independent experiments. (inset) Fluorescence (fluo) of 125 nM [NBD]α-synuclein as a function of phospholipid concentration. Color coding for sonicated and extruded liposomes is indicated on the left. Calculation of partition coefficients is described in Materials and methods. (C) Sequence of the AH region of α-synuclein highlighting the repeating character of this region, which can be divided into 11-mer repeats. The mutations harbored by the T6 mutant consist in replacing all threonine residues (pink; left) of the nonpolar region by a more hydrophobic residue (Leu or Phe, yellow; right). Position of mutated residues in the 11-mer repeats is boxed (wild type; left) or shaded (mutant; right). Color coding is as in Fig. 2; in the alignment only mutated and charged residues are colored. (D) Binding of T6 mutant α-synuclein to small liposomes containing increasing amounts of POPS at the expense of POPC as in A. (E) Binding of T6 mutant α-synuclein to size-calibrated charged liposomes as in B. Concentrations in A, B, D, and E of proteins were 125 nM and phospholipids were 150 μM. Data in A and D were fitted (dashed lines) to a sigmoidal function ($y = a + bx^n/(c + x^n)$). The dashed lines in B and E were simply used to illustrate the apparent shape of the curve for binding as a function of liposome radius.

seen on a helical projection, are positioned right in the middle of the hydrophobic face (Fig. 3 C). Threonine, although generally considered as a polar residue, has some hydrophobic character because of its methyl group. Replacing each threonine by a phenylalanine or a leucine should considerably increase the hydrophobicity of the nonpolar face. The lipid-binding properties of the sextuple T6 mutant was assessed using the same liposomes as those used for the wild-type form, that is, liposomes of fixed size and varying amounts of POPS or liposomes of varying size and a fixed amount of POPS. The sextuple mutation changed completely the lipid-binding properties of α-synuclein. Whereas the wild-type form exhibited strong dependencies on both liposome charge and membrane curvature (Fig. 3, A and B), the T6 mutant bound to all liposomes regardless of the amount of POPS present and on the size of the liposome (Fig. 3, D and E). One striking observation was that the T6 mutant could even bind efficiently to large neutral liposomes (Fig. S3 A), which have the most unfavorable features for the binding of wild-type α-synuclein. These results demonstrate that the poor hydrophobic face of the α-synuclein AH is required for both its curvature-sensing capacity and its sharp dependency on anionic lipids.

To examine the in vivo properties of the T6 α-synuclein mutant, we expressed this mutant in yeast cells. Wild-type α-synuclein localizes to the PM in addition to vesicular structures (Fig. 1, C and G), as has been shown previously (Auluck et al., 2010). PM binding is mediated by the C-terminal region of α-synuclein and is likely caused by protein–protein interactions with PM-localized proteins (see following section of Results). Strikingly, only ∼2% of yeast cells expressing the T6 mutant had vesicular structures, in contrast to more than 40% of cells expressing wild-type α-synuclein (Fig. S3, B and C). T6 α-synuclein localized primarily to the PM, indicating strong targeting to membranes (Fig. S3, C and D). Hence, the capacity

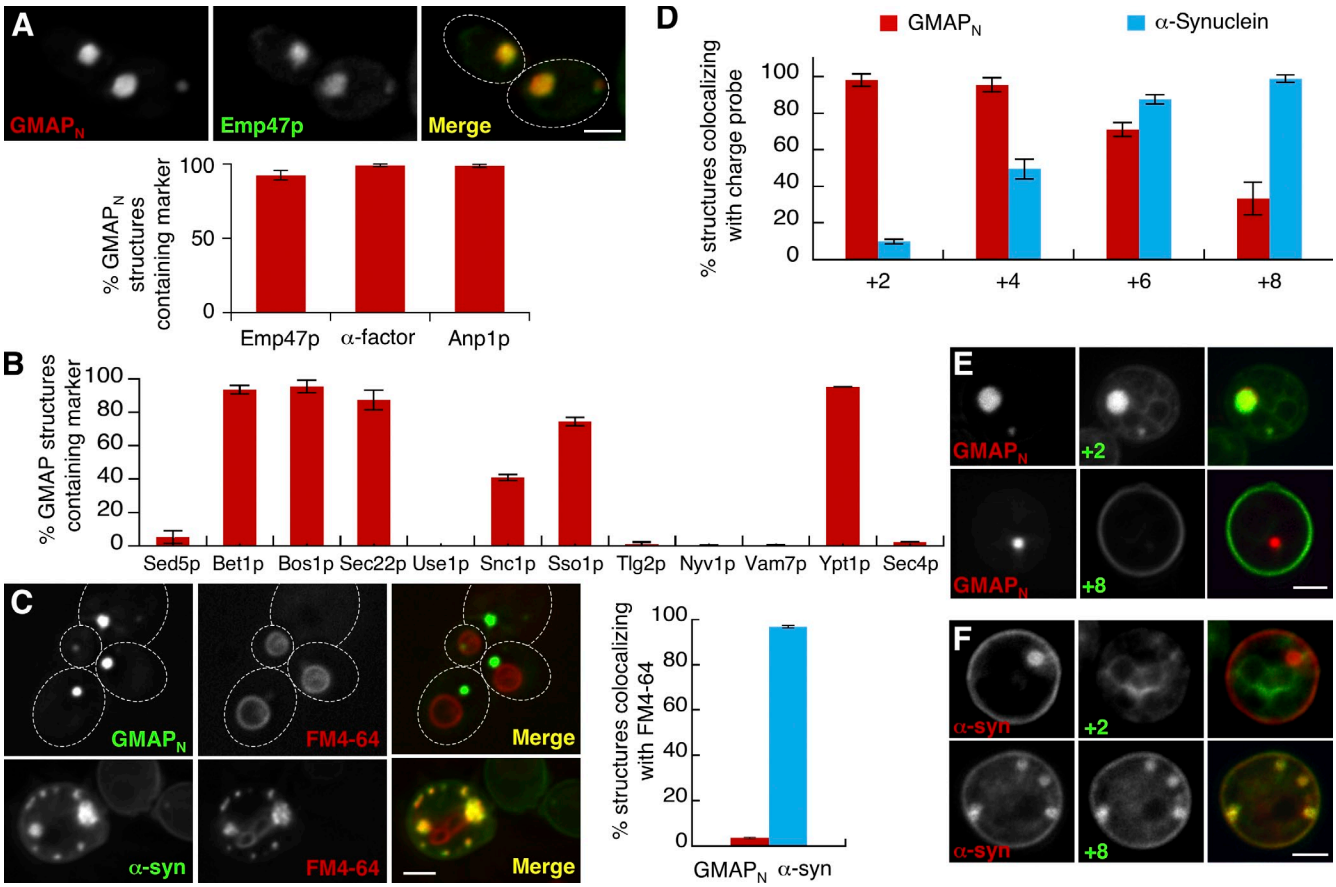


Figure 4. **GMAP$_N$ and α-synuclein structures colocalize with distinct compartment markers in yeast.** (A) Localization in SEY6210 cells of GMAP$_N$-mCherry with either GFP-Emp47p or pro–α-factor–citrine and of Anp1p–monomeric RFP (mRFP) with GMAP$_N$-GFP. (top) Representative images of colocalization of GMAP$_N$-mCherry and GFP-Emp47p. (bottom) For quantifications, between 30 and 100 GMAP$_N$ structures were scored for the presence or absence of the cargo protein, and percentages were calculated (see Materials and methods). (B) Localization in SEY6210 cells of GMAP$_N$-mCherry with the indicated GFP-tagged protein. Quantifications were performed as in A. (C) Localization in BY4742 of GMAP$_N$-GFP or α-synuclein–GFP (α-syn) with FM4-64. (D–F) Localization in BY4742 of GMAP$_N$-mCherry or α-synuclein–mCherry with GFP-tagged charge probes carrying the indicated number of lysine residues. Quantifications (D) and representative images (E and F) are shown. Cells were grown overnight at 23°C (A–C) or 16°C (D–F) under inducing conditions, and then, live cells were imaged and quantified. Means and SDs of at least three independent experiments are shown. Outlines of cells are indicated by dashed lines. Bars, 2 µm.

of α-synuclein to sense membrane curvature, caused by the unbalanced nature of its AH, is important for its ability to accumulate clusters of vesicles in yeast cells.

### GMAP$_N$ and α-synuclein colocalize with different membrane markers in yeast cells

To determine whether GMAP$_N$ structures contain COPII or COPI vesicles, we tested colocalization with their cargo molecules, including the ER-Golgi cargo receptor Emp47p, the COPII vesicle cargo pro–α-factor, and the cis-Golgi enzyme Anp1p (Wooding and Pelham, 1998; Lee et al., 2004). A high percentage of GMAP$_N$ structures contained these markers (Figs. 4 A and S4 A). However, colocalization experiments with subunits of the COPII and COPI coats, as well as with clathrin, revealed little, if any, overlap with GMAP$_N$ (Fig. S4, B and C), supporting the conclusion that they are made up of uncoated vesicles. Three ER-Golgi SNAREs (Bos1p, Bet1p, and Sec22p) were present in a large fraction of GMAP$_N$ structures, but the fourth member of this SNARE complex, Sed5p, was not (Fig. 4 B). GMAP$_N$ structures did not contain endosomal or vacuolar SNAREs, but a significant proportion did contain Snc1p and Sso1p, which mediate fusion of secretory vesicles with the PM (Fig. 4 B). Colocalization with GMAP$_N$ could either be caused by their presence as cargo in COPII vesicles or to the presence of late secretory vesicles in GMAP$_N$ structures. The former hypothesis is strongly supported by the fact that Sec4p, a Rab protein localized to post-Golgi secretory vesicles, did not colocalize with GMAP$_N$ to a significant extent, whereas most GMAP$_N$ structures did contain the early Golgi Rab Ypt1p (Fig. 4 B). Hence, GMAP$_N$ structures contain markers specific to vesicles of the early secretory pathway.

Given the proximity of α-synuclein structures to the cell periphery, we tested whether they colocalized with peripheral ER, using the reticulon Rtn1p as a marker of this compartment (Voeltz et al., 2006). Although α-synuclein structures were adjacent to Rtn1p patches at the cell periphery, there was little, if any, overlap (Fig. S4, B and C). To determine whether α-synuclein or GMAP$_N$ structures contain endocytic membranes, cells were treated with FM4-64, a marker of the endocytic pathway. GMAP$_N$ structures did not colocalize with FM4-64, even after long chase

times, at which point the dye was localized primarily to vacuoles (Fig. 4 C). In contrast, α-synuclein structures almost all contained FM4-64–labeled membranes (Fig. 4 C).

Surface charge biosensors, farnesylated peptides that contain varying numbers of positively charged amino acids fused to GFP, bind to membranes of different levels of negative charge (Yeung et al., 2008). When coexpressed with $GMAP_N$ or α-synuclein, opposite colocalization patterns were observed. Almost all $GMAP_N$ structures colocalized with the +2 probe with progressively fewer containing the more highly charged probes (Fig. 4, D and E). In contrast, only a small fraction of α-synuclein structures contained the +2 probe, whereas essentially all contained the +8 probe (Fig. 4, D and F). Because α-synuclein binds to PS-containing vesicles in vitro, we tested the PS-specific probe LactC2 (Yeung et al., 2008) and found that it colocalized to a high level with α-synuclein but not with $GMAP_N$ (Fig. S4 D). These results support the conclusion that in cells, as in vitro, α-synuclein preferentially binds to negatively charged membranes, whereas $GMAP_N$ does not require a charge for membrane binding.

### The ALPS motif and the N-terminal region of α-synuclein act as localization determinants in yeast cells

The ALPS motif of $GMAP_N$ is required for its localization in yeast cells because deleting it renders the truncated protein cytosolic (Fig. 5 A). In contrast, when the CC region of $GMAP_N$ (aa 39–377) was replaced with a portion of the CC of the nuclear cohesin Smc1p (Haering et al., 2002), membrane targeting was not affected. The CC of Smc1p on its own localized primarily to the nucleus, but when the ALPS motif was appended to the N terminus, the chimeric protein was localized to cytoplasmic puncta (Fig. 5 B). EM analysis indicated that cells expressing this ALPS–Smc1-CC chimera contained accumulations of vesicles (Fig. 5 C). Hence, the GMAP-210 ALPS motif acts as a localization determinant in yeast cells and is responsible for the accumulation of vesicular structures.

Comparison of $GMAP_N$ and α-synuclein localization is complicated by their different structures: $GMAP_N$ is a CC dimer presenting two copies of a 38-aa-long AH, whereas α-synuclein is a monomer with a 90-aa-long AH and an acidic tail. To create a perfectly matched pair, we constructed a chimera in which the 38-aa ALPS motif of $GMAP_N$ was replaced with the first 38 aa of α-synuclein (Fig. 6 A). The α-synuclein chimera was found in patches of fluorescence at the cell periphery (Fig. 6 A, right), in striking contrast to the randomly dispersed cytoplasmic puncta in cells expressing $GMAP_N$ (Fig. 6 A, left). Like full-length α-synuclein, and unlike $GMAP_N$, the chimera colocalized to a very high level with the endocytic marker FM4-64, and α-synuclein chimera structures did not overlap Rtn1p structures (Fig. 6, B and C). In addition, we found a high percentage of chimera structures colocalizing with the fluid phase marker Lucifer yellow, another marker of the endocytic pathway (Fig. 6, B and C). Also like α-synuclein, the α-synuclein chimera did not colocalize with coats (Fig. S4 E), and its expression severely inhibited yeast growth (Fig. 6 D). Like α-synuclein, and unlike $GMAP_N$, expression of the α-synuclein chimera caused a slowing of endocytosis (Fig. 6 E). Examination of cells expressing the α-synuclein chimera by EM revealed striking accumulations of small vesicles at the cell periphery (Fig. 6, F and G). Vesicles were present in structures closely juxtaposed to the PM (Fig. 6 F) and, in some cells, were found in a single layer along the PM at a fixed distance (Fig. 6 G).

### The α-synuclein chimera specifically colocalizes with endocytic and post-Golgi vesicle markers

Although we found significant differences in colocalization patterns between $GMAP_N$ and α-synuclein, we also found a lack of specificity in the membranes accumulated within α-synuclein structures (Fig. S5 A) as has been reported previously (Gitler et al., 2008; Soper et al., 2011). These results imply either that α-synuclein binds nonspecifically to many types of vesicles in cells or that it binds specifically to one class of vesicle, and colocalization with other markers is a secondary effect. Experiments with the α-synuclein chimera support the latter hypothesis. In contrast to full-length α-synuclein, the chimera structures did not contain either the early endosomal SNARE Tlg2p or the ER SNARE Use1p (Fig. S5 B). At early time points after induction, <5% of the α-synuclein chimera structures colocalized with early Golgi markers (Fig. 7, A and C). In contrast, Snc1p and the endocytic marker FM4-64 colocalized with the α-synuclein chimera to a high level, even after short periods of induction (Figs. 7, B and C; and S5 B). At early time points after induction, ∼40% of α-synuclein chimera structures contained the secretory vesicle marker Sec4p, and Ypt1p was present in 70–80% of chimera structures, likely because of its role in trafficking within the endocytic pathway (Sclafani et al., 2010).

We examined the localization of the α-synuclein chimera in several endocytosis mutants and found a marked effect in *sla2Δ* cells. In *sla2Δ* mutants, there is a dramatic slowing of the internalization step of endocytosis, and scission of endocytic vesicles is blocked (Kaksonen et al., 2003). Many *sla2Δ* cells did not accumulate chimera-GFP–labeled structures, and those that did had significantly fewer structures than in wild-type cells (Fig. S5 C).

As described previously (Auluck et al., 2010), α-synuclein localizes to the PM in addition to vesicular structures, but we did not observe PM localization of the α-synuclein chimera (Figs. 6 and 7). α-Synuclein interacts with protein partners, including the synaptic vesicle SNARE synaptobrevin, via its acidic C terminus (Auluck et al., 2010; Burré et al., 2010). In coimmunoprecipitation experiments, we found that the α-synuclein chimera did not interact with the yeast homologue of synaptobrevin, Snc1p, whereas full-length α-synuclein did (Fig. S5 D), supporting the conclusion that protein–protein interactions contribute to PM localization of full-length α-synuclein in yeast.

### Membrane targeting mechanism in cells

To address the question of whether targeting of $GMAP_N$ and the α-synuclein chimera to distinct membranes occurred through protein–protein or protein–lipid interactions in cells, we used several approaches. Previous work has shown that

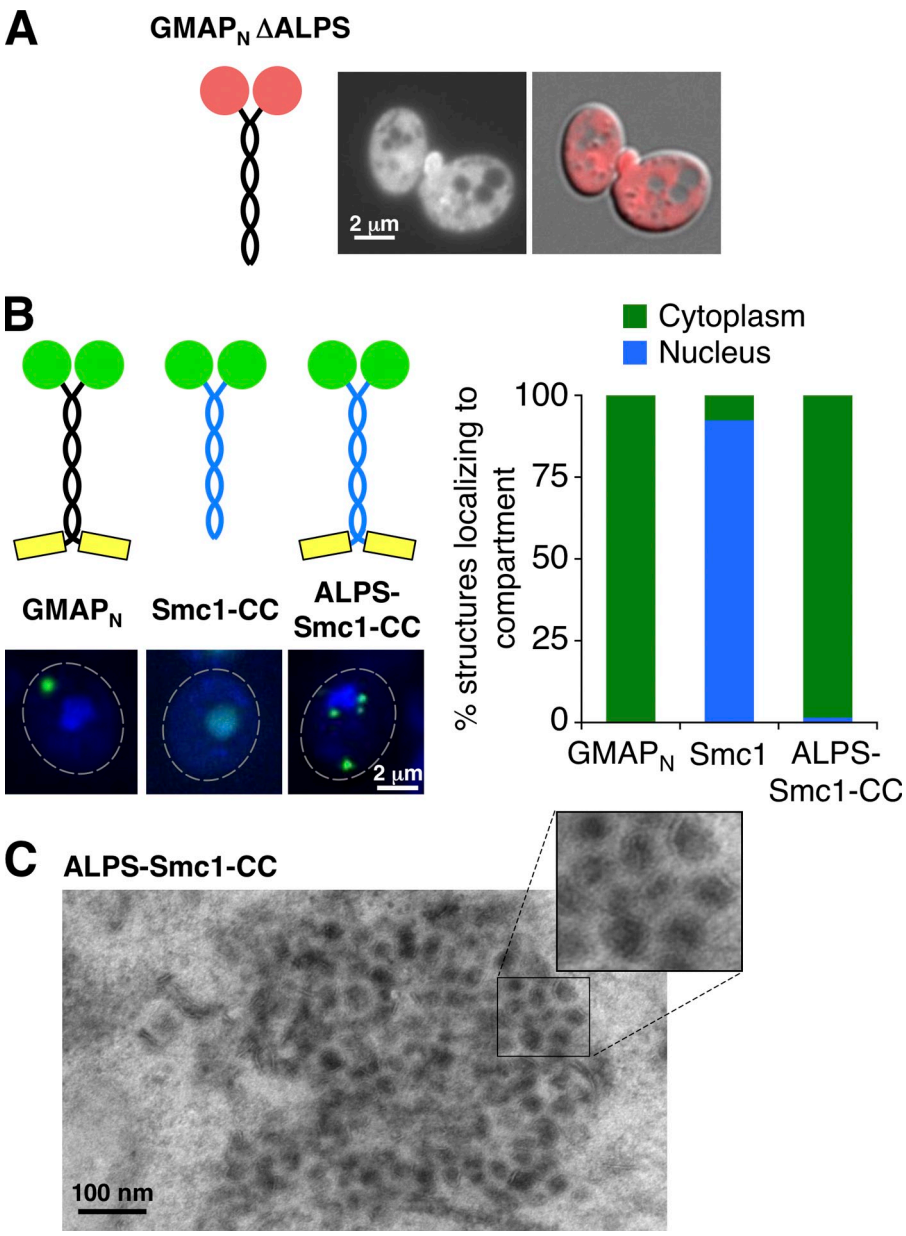


Figure 5. **The ALPS motif of GMAP-210 acts as a localization determinant to cytoplasmic vesicular structures.** (A) Localization of a truncated version of GMAP$_N$-mCherry with the ALPS motif deleted (schematic diagram, left). Fluorescence (left) and overlay onto a differential interference contrast image (right) are shown. (B, left) Localization (bottom) of constructs is shown in the schematic diagrams (top). ALPS–Smc1-CC was constructed by replacing the CC region of GMAP$_N$ with that of the nuclear protein Smc1p (aa 158–374). (right) For quantifications, 60–130 structures for each GFP fusion protein were scored for localization to the nucleus, as visualized by Hoechst staining, or to the cytoplasm. Results shown are representative of two independent experiments. Outlines of cells are indicated by dashed lines. (C) Representative EM image of cells expressing the ALPS–Smc1-CC–GFP chimeric protein. Inset shows a higher magnification of the boxed region. BY4742 cells expressing the indicated proteins were grown overnight under inducing conditions before imaging.

α-synuclein and proteins containing ALPS motifs can interact with SNARE proteins (Rein et al., 2002; Burré et al., 2010; Thayanidhi et al., 2010), and both GMAP$_N$ and α-synuclein chimera vesicular structures colocalized with SNAREs (Figs. 4 B and 7). However, our attempts to coimmunoprecipitate ER–Golgi SNAREs and GMAP$_N$ from yeast cells were unsuccessful, suggesting that there is not a strong interaction between them. Similar results were obtained for the α-synuclein chimera and Snc1p (Fig. S5 D). Next, we introduced mutations into GMAP$_N$ that altered the amphipathic nature of the ALPS motif, either by insertion of two residues to produce a register shift or by mutation of hydrophobic residues to alanines or aspartates. All of these mutations in GMAP$_N$ resulted in a diffuse cytosolic localization pattern (Table I), indicating that the amphipathic properties of the ALPS motif are required for localization to vesicular structures in yeast cells. Finally, we tested the localization of a GMAP$_N$ construct in which the ALPS motif was replaced by its inverted sequence (invALPS-GMAP; Fig. 8). We reasoned that if the ALPS motif is localized via a protein–lipid interaction, inverting the sequence of the ALPS motif should not affect its capacity to localize to vesicles in cells because the chemical features of the AH are preserved (Fig. 8 A). Such an inversion should, however, compromise protein–protein interactions, as the inverted sequence shares little homology with the original ALPS sequence.

Cells expressing invALPS-GMAP accumulated structures to the same extent and in a cellular distribution identical to that of GMAP$_N$ (Fig. 8, B and C). These structures were composed of small vesicles, indistinguishable from those found in cells expressing the original GMAP$_N$ protein (Fig. 8 B). Importantly, the ER–Golgi cargo receptor Emp47p and ER–Golgi SNAREs Sec22p and Bet1p colocalized to the same extent with the invALPS-GMAP structures as they did with wild-type GMAP$_N$, whereas invALPS-GMAP structures did not colocalize with

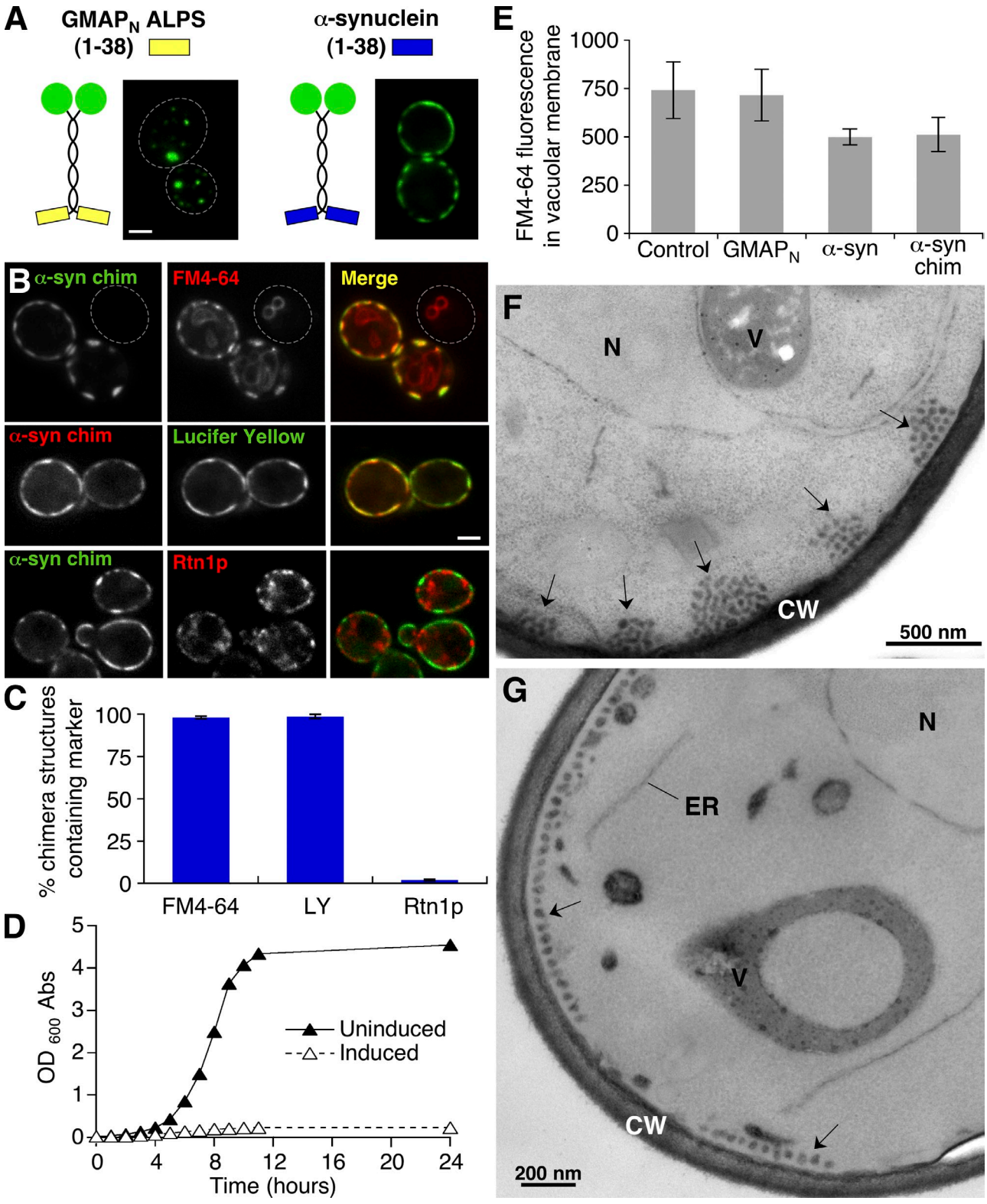


Figure 6. **The first 38 aa of α-synuclein act as a localization determinant to peripheral vesicular structures containing endosomal markers.** (A) Schematic diagrams of the GMAP$_N$-GFP and α-synuclein chimera–GFP probes and their localization in yeast cells. (B) Localization of α-synuclein chimera–GFP (α-syn chim) with FM4-64 (top) and Rtn1p-mRFP (bottom) and of α-synuclein chimera–mCherry with Lucifer yellow (LY; middle). (A and B) Bars, 2 µm. (C) Quantifications of the experiments shown in B. (D) Strain IPY6 α-synuclein chimera–GFP was grown overnight under repressing conditions and then shifted (open symbols) or not shifted (closed symbols) to induction medium for the indicated times, and absorbance (Abs) of the cultures at $OD_{600}$ was monitored. (E) BY4742 cells expressing the indicated constructs were grown overnight under inducing conditions and treated with FM4-64, and the level of fluorescent signal in vacuolar structures was determined as described in Materials and methods. (F and G) Representative EM images of BY4742 cells expressing α-synuclein chimera–GFP induced for 16 h. Arrows show vesicular structures. N, nucleus; V, vacuole; CW, cell wall. Means and SDs of at least three independent experiments are shown.

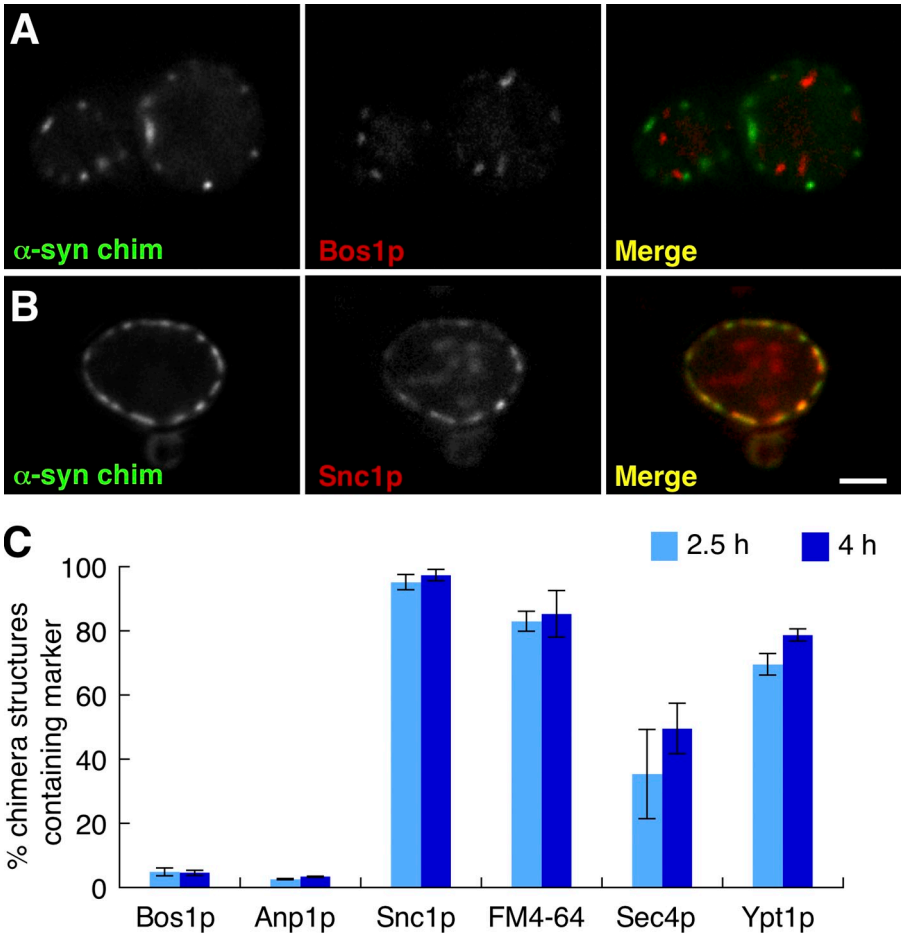


Figure 7. **The α-synuclein chimeric probe colocalizes specifically with endocytic and post-Golgi markers.** (A–C) Localization of the α-synuclein chimera–GFP (α-syn chim) with the indicated mCherry-tagged marker. Representative images for mCherry-Bos1p (A) and mCherry-Snc1p (B) are shown. Quantifications are depicted in C. Cells were grown overnight under repressing conditions and then transferred to induction medium for 2.5 (A–C) or 4 h (C). Means and SDs of at least three independent experiments are shown. Bar, 2 µm.

the endocytic marker FM4-64 at early time points after induction (Fig. 8, C and D). Hence, the capacity to cause accumulations of early secretory pathway vesicles in yeast cells is not dependent on the orientation of the ALPS motif sequence. Together, these results support the conclusion that localization of $GMAP_N$ to vesicular structures in yeast occurs primarily through protein–lipid interactions.

## Discussion

The discovery of membrane curvature sensors revealed that membrane trafficking could be regulated by membrane shape. Studies to date have focused on the principle that membrane curvature directs the binding of these sensors to lipid vesicles (McMahon and Gallop, 2005; Hatzakis et al., 2009; Drin and Antonny, 2010; Liu et al., 2010). Whether curvature sensors have the capacity to discriminate between membranes of different lipid composition is less well explored. Here, we have compared the lipid-binding properties of two amphipathic curvature sensors whose chemistries are strikingly different: an ALPS motif and α-synuclein (Fig. 2, A and B). Comparison of their lipid-binding properties in vitro confirms that this difference in chemistry translates into specific binding to liposomes of different composition, complementary to the chemical properties of each curvature sensor. Remarkably, when expressed in yeast cells, these mammalian curvature sensors specifically target distinct classes of vesicles, with properties corresponding to their preferred in vitro lipid environment.

Table I. **Localization of $GMAP_N$ mutants in yeast cells**

| Protein expressed | Mutations | Expression level | Localization |
|---|---|---|---|
| $GMAP_N$ (aa 1–375) | None | WT | Cytoplasmic puncta (EM; vesicle accumulations) |
| $GMAP_N$ (aa 1–375) | ALPS L8A | WT | Diffuse cytoplasmic |
| $GMAP_N$ (aa 1–375) | ALPS W4A L5A | ≥WT | Diffuse cytoplasmic |
| $GMAP_N$ (aa 1–375) | ALPS L23D L26D | ≥WT | Diffuse cytoplasmic |
| $GMAP_N$ (aa 1–375) | ALPS ins25AA | WT | Diffuse cytoplasmic |
| $GMAP_N$ (aa 1–375) | ALPS ins25DD | WT | Diffuse cytoplasmic |
| $GMAP_N$ (aa 39–375) | ΔALPS (Δ1–38) | ≥WT | Diffuse cytoplasmic (EM; no vesicles accumulated) |
| $GMAP_N$ (aa 1–160) | CC truncation (Δ161–377) | WT | Cytoplasmic puncta (EM; vesicle accumulations) |

WT, level of wild-type $GMAP_N$ after overnight induction.

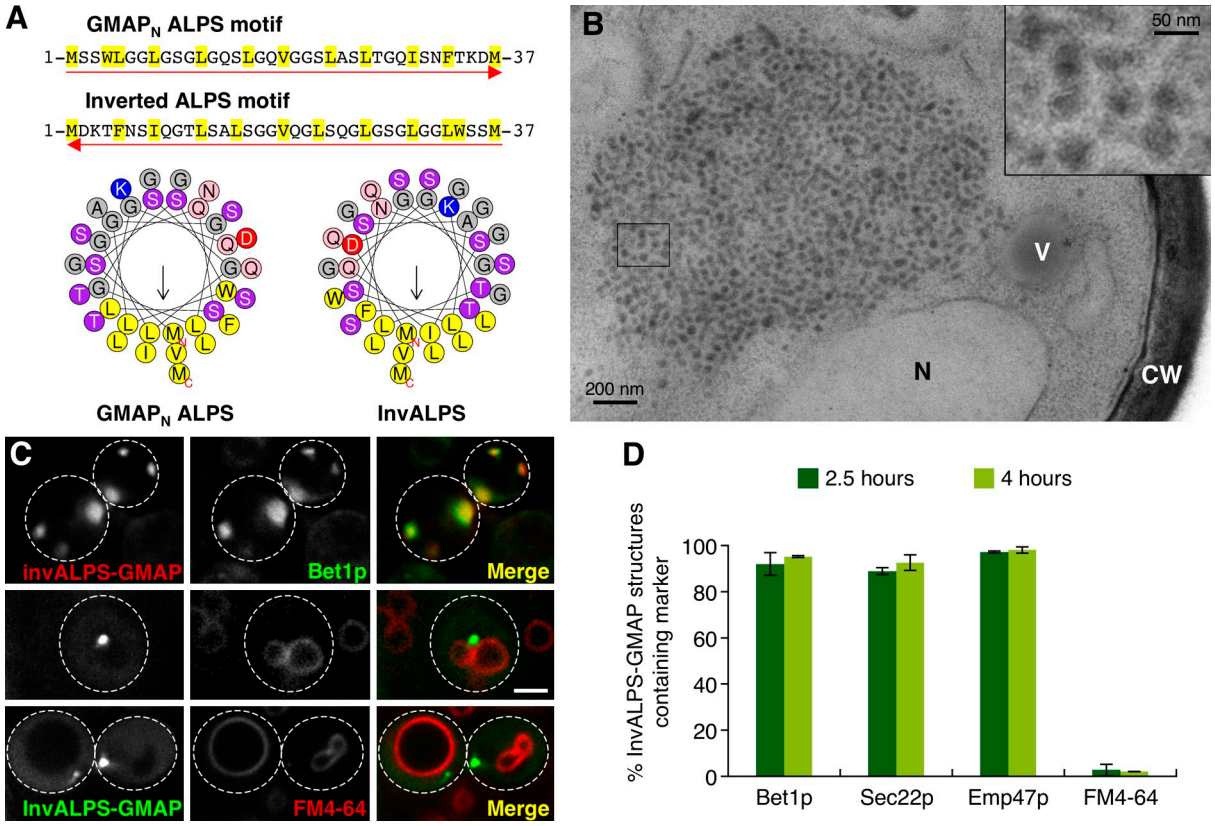


Figure 8. **Inverting the ALPS motif sequence does not affect the capacity of GMAP$_N$ to accumulate early secretory pathway vesicles.** (A) The GMAP-210 ALPS motif sequence and its inverted sequence (top) and their helical wheel representations (bottom). Yellow: Val, Leu, Ile, Met, Phe, and Trp. Pink: Ser and Thr. Red: Asp and Glu. Blue: Lys and Arg. Grey: other residues. (B) Representative EM image of cells expressing invALPS-GMAP. Inset shows boxed region at a higher magnification. N, nucleus; V, vacuole; CW, cell wall. (C) Localization of invALPS-GMAP–mCherry with GFP-Bet1p after 4 h of induction (top) and of invALPS-GMAP–GFP with FM4-64 after 2.5 h of induction (bottom). Bar, 2 µm. (D) Quantification of localization of invALPS-GMAP–mCherry with GFP-Bet1p, GFP-Sec22p, or GFP-Emp47p or of invALPS-GMAP–GFP with FM4-64 at the indicated times after induction. SEY6210 (or BY4742 for FM4-64 imaging) cells carrying the indicated proteins on plasmids were grown overnight under inducing conditions (B) or overnight under repressing conditions and shifted to induction medium for 2.5 or 4 h (C and D). Means and SDs of at least three independent experiments are shown. Outlines of cells are indicated by dashed lines. N, N terminus; C, C terminus.

The mechanisms by which ALPS motifs and α-synuclein sense membrane curvature are on the one hand similar and on the other hand opposite. The similarity relies on the strong unbalance between the polar and nonpolar face, which exacerbates the need for positive membrane curvature. In other words, both GMAP$_N$ and α-synuclein have a weakness that makes positive membrane curvature mandatory for their binding, probably because membrane curvature facilitates the insertion of the AH into the membrane interfacial region. However, what renders their lipid binding opposite is the fact that α-synuclein uses electrostatic interactions to overcome the minimal contribution of its hydrophobic face, whereas an ALPS motif relies on the hydrophobic force to compensate for its lack of charged polar residues.

The lipid binding of both ALPS motifs and α-synuclein depends very sharply on liposome size, a property that we propose is caused by the length and repetitive nature of the AHs formed by these two proteins (Antonny, 2011). For an AH of $n$ turns, if each turn has the same equilibrium constant $K$ for the coupling between folding and adsorption, the equilibrium constant for the adsorption of the entire AH will depend on $K^n$. This repetitive mode of membrane interaction, akin to Velcro, can amplify small differences in the lipid-binding properties of each fundamental unit. Hence, the dimer of GMAP-210 ALPS motifs and α-synuclein, both of which have >20 helical turns, have a high capacity to sense the subtle differences in lipid packing that differentiate highly curved and flatter membranes.

Given the very different chemistries of the AHs formed by ALPS motifs and α-synuclein, they are ideally suited to sensing the different lipid compositions of their target vesicles directly. Inversion of the ALPS motif sequence, which preserves specific membrane targeting but should compromise any potential protein–protein interactions, provides strong support for this conclusion. Both secretory vesicles (Zinser et al., 1991; Klemm et al., 2009) and endocytic vesicles (Sun et al., 2007) in yeast, as in other eukaryotes, have high levels of anionic phospholipids, in contrast to vesicles of the early secretory pathway trapped by the GMAP$_N$ ALPS motif. Hence, the properties of the vesicles that α-synuclein and ALPS motifs associate with in cells correlate well with their in vitro lipid-binding properties, particularly in terms of charge (Figs. 2 and 4 D). The differences in the hydrophobic faces of ALPS motifs and α-synuclein might also aid in their discrimination of different types of vesicles. ALPS motifs should have a preference for the unsaturated lipids of the early secretory pathway, whereas α-synuclein with its

small hydrophobic face should be accommodated well in membranes with higher levels of saturated phospholipids. This aspect awaits further investigation.

The AHs formed by the GMAP-210 ALPS motif and α-synuclein represent two extremes of AH structure. Other AHs with distinctive chemistries are also adapted to specific cellular membranes. The N-terminal AH of epsin, along with residues in the adjacent epsin N-terminal homology domain, make direct contacts with phosphatidylinositol 4,5-bisphosphate (Ford et al., 2002). The autoinhibitory AH of CTP:phosphocholine cytidylyltransferase binds to and inhibits the catalytic domain of the enzyme and is displaced by binding to membranes only when their PC content drops below a critical level (Cornell and Taneva, 2006). Spo20p, a PM SNARE in yeast, has an N-terminal AH that acts as a sensor of phosphatidic acid–enriched membranes (Nakanishi et al., 2004; Liu et al., 2007). The fact that AHs penetrate into the interfacial region of the bilayer, where they interact with multiple lipids, allows them to integrate many physicochemical parameters of cellular membranes (Antonny, 2011).

AHs also differ in their ability to sense or induce membrane curvature. That ALPS motifs and α-synuclein are sensing, rather than inducing, vesicles in yeast cells is supported by several observations. In cells expressing these proteins, we observed no increase in the frequency of tubules or budding profiles (Figs. 1 and 6). We estimated that the ratio of $GMAP_N$ protein to phospholipid is ∼1:1,000 in yeast cells, a ratio at which $GMAP_N$ does not induce membrane deformations in vitro (Drin et al., 2008). If α-synuclein was able to form membrane vesicles, the α-synuclein T6 mutant, with the increased hydrophobicity of its nonpolar face, should be even more efficient at doing so. However, we found exactly the opposite result: yeast cells expressing this mutant accumulated many fewer vesicular structures (Figs. 3 and S3). Collectively, our results are most consistent with the idea that ALPS motifs and α-synuclein are curvature sensors both in vitro and in vivo. It is likely that high levels of these curvature sensors in cells prevent vesicle fusion but not tethering, leading to formation of vesicle clusters, a mechanism recently described for clustering of secretory vesicles in yeast (Rossi and Brennwald, 2011).

We demonstrated a high level of specificity in α-synuclein membrane targeting in yeast cells through the construction of a novel α-synuclein chimeric probe, based on the design principle of $GMAP_N$, in which the 38-aa ALPS motif was replaced with the first 38 aa of α-synuclein. As previously described by other groups (Auluck et al., 2010), we observed localization of α-synuclein to the PM in addition to vesicular structures. Given the strong selectivity of α-synuclein for small liposomes in vitro, it is unlikely that localization to the relatively flat PM is mediated solely by lipid interaction of its AH and may involve the C-terminal region, which is known to interact with protein partners (Auluck et al., 2010; Burré et al., 2010). Strong support for this conclusion comes from the fact that the α-synuclein chimera did not localize to the PM but only to vesicular clusters closely juxtaposed to the PM (Figs. 6 and 7). Most of these structures contained Snc1p, the yeast homologue of VAMP/synaptobrevin, whose mechanism of trafficking is conserved from yeast to humans (Burston et al., 2009). Hence, α-synuclein likely traps endocytic vesicles containing Snc1p in yeast and may have a similar function in neurons, in which it has been reported to regulate synaptic vesicle recycling (Ben Gedalya et al., 2009; Nemani et al., 2010).

Expression of $GMAP_N$ and the α-synuclein chimera in yeast led to accumulation of vesicles that appeared to be blocked before fusion but after uncoating, suggesting that these curvature sensors might be involved in regulating a late step in vesicle fusion. α-Synuclein has been shown to promote assembly of synaptic vesicle SNARE complexes (Burré et al., 2010), which is consistent with the idea that it regulates synaptic vesicle fusion. The probes we have described here should provide useful tools to explore mechanisms by which curvature sensors might regulate fusion of the vesicles that they are targeted to.

## Materials and methods

### Yeast strains, plasmids, and antibodies

Yeast strains used in this study are shown in Table S1. To optimize $GMAP_N$ expression in yeast, a synthetic gene was constructed in which all codons were changed to those most optimal for yeast. $GMAP_N$, α-synuclein, and the α-synuclein chimera (α-synuclein aa 1–38 fused to aa 39–375 of $GMAP_N$) were fused to yeast EGFP (yEGFP; Cormack et al., 1997), expressed under the control of the $TetO_2$ promoter in pAP90 (a gift from A. Peyroche, Commissariat à l'Energie Atomique, Gif-sur-Yvette, France), resulting in plasmids pIP7, pIP29, and pIP119. pIP90, pIP12, and pIP148 were constructed by transferring the $TetO_2$ promoter cassettes of pIP7, pIP29, and pIP119 into pRS306 and were integrated at the *URA3* locus in SEY6210 to generate IPY1, IPY2, and IPY3, respectively. pIP152, pIP153, and pIP156 were constructed by first replacing the 3HA tag between sites PacI and AscI of pFA6a-His3MX6-PGAL1-GFP-3HA (Longtine et al., 1998) with the genes encoding $GMAP_N$–, α-synuclein–, and α-synuclein chimera–yEGFP fusions, to place the mammalian yEGFP fusions downstream of the PGAL1 promoter. These PGAL1-X–yEGFP cassettes were cloned into pFA6a-GFP(S65T)-HIS3, replacing the GFP(S65T) gene with PGAL1-X–yEGFP. PCR products from reactions using oligonucleotides targeting integration to the intergenic region between *GAL1* and *GAL10*, with pIP152, pIP153, or pIP156 as templates, were transformed into strains IPY1, IPY2, and IPY3 to generate IPY4, IPY5, and IPY6. Strains were grown in YPD (yeast extract peptone dextrose) medium with 10 µg/ml doxycycline to repress expression and induced in YP + 2% galactose.

pIP30 and pIP122 carry mCherry versions of $GMAP_N$ and the α-synuclein chimera, respectively, in pAP901, derived from pAP90 by replacement of yEGFP with mCherry. pIP71 and pIP61 carry mCherry fusions of $GMAP_N$ and α-synuclein under control of the $TetO_2$ promoter in pRS425 (2µ LEU2). pIP66 carries $GMAP_N$-mCherry under control of the $TetO_7$ promoter in pCM252 (CEN [centromeric vector] *TRP1*; Bellí et al., 1998). pCM188 and pCM252 were gifts from E. Herrero (Universitat de Lleida, Lleida, Spain), and mCherry-N1 was a gift from G. Patterson (National Institute of Biomedical Imaging and Bioengineering, Bethesda, MD). A portion of the Smc1p CC (aa 158–374; a gift from D. Koshland, Carnegie Institution, Baltimore, MD) and the ALPS motif of GMAP-210 fused its N terminus (ALPS–Smc1-CC), deletion and point mutants of $GMAP_N$, and the inverted ALPS sequence fused to GMAP-210 aa 39–375 (invALPS-GMAP) were expressed as yEGFP fusions in plasmids derived from pAP90. pIP130 carries invALPS-GMAP–mCherry in pAP901. Genes encoding Sec4p, Ypt1p, and SNAREs were cloned with yEGFP or mCherry at their N termini in pCM252. pIP108–pIP112 were constructed by transferring LactC2 (Yeung et al., 2008) and +2, +4, +6, and +8 charge probes (Roy et al., 2000; gifts from J. Silvius, McGill University, Montréal, Québec, Canada) into pAP90. To repress expression, yeast transformants were grown in selective minimal medium with 2% glucose and 10 µg/ml doxycycline; to induce expression, the same medium without doxycycline was used. pKSY142 GFP-Emp47p (Sato and Nakano, 2003) and yeast enhanced citrine-tagged glycosylated pro–α-factor (Castillon et al., 2009) were gifts from K. Sato (University of Tokyo, Tokyo, Japan) and H. Riezman (University of Geneva, Geneva, Switzerland). Mutagenesis was performed using a site-directed mutagenesis kit (QuickChange II XL; Agilent Technologies). All plasmids constructed in this study were confirmed by DNA sequencing.

The plasmids expressing the $GMAP_N$ mutants shown in Table I were derived from pIP7. Transformants were induced overnight, and the level of each mutant protein was compared with that of $GMAP_N$ by Western blot analysis. Mouse monoclonal antibodies GMAP-210/TRIP11 (BD), GFP (Roche), carboxypeptidase Y (CPY; Invitrogen), and α-synuclein (BD) were used for Western blot analysis, and purified rabbit polyclonal GFP (Abcam) was used for immuno-EM.

**$GMAP_N$ purification and labeling**

The N-terminal region of GMAP-210 (aa 1–375; $GMAP_N$) carrying the M1C mutation and lacking the four endogenous cysteines (mutations C75L, C212S, C350L, and C357L) was expressed in *Escherichia coli* at 17°C in the form of a GST fusion (pGEX-4T2 vector). The fusion protein was purified from the bacterial soluble fraction using glutathione beads. After thrombin cleavage, the 1–375-aa fragment was labeled with a fivefold molar excess of NBD iodoacetamide (Invitrogen) from a stock solution in dimethyl formamide (DMF; final DMF volume <5%). The labeled protein was further purified by gel filtration chromatography on a Sephacryl S-300 column. The final purified product was analyzed by mass spectroscopy and N-terminal sequencing, which confirmed the mutations and labeling.

**α-Synuclein mutagenesis, purification, and labeling**

α-Synuclein cloned into vector pET21b (not including the His6 tag) and containing the V3C mutation was expressed in *E. coli* (0.5-liter culture) and purified from the soluble fraction by a standard procedure that includes a 15-min boiling step to precipitate other proteins. After centrifugation, the supernatant, which contained mostly α-synuclein (in the range of 100 µM), was incubated with a fivefold molar excess of NBD iodoacetamide from a stock solution in DMF (DMF volume <5%). After incubation at room temperature for 10 min and in the dark, 5 mM cysteine was added to quench the excess dye. The sample was then dialyzed on a NAP-10 column and further purified by 40 ml Q Sepharose chromatography using a NaCl gradient (0–1 M). The peak of α-synuclein was 95% pure and, according to UV-visible absorption spectroscopy, was 100% labeled with NBD. The final purified product was analyzed by mass spectroscopy and N-terminal sequencing, which confirmed the mutations and labeling.

The T6 form of α-synuclein contains six mutations (T22L, T33F, T44L, T59L, T81F, and T92L) in addition to the V3C mutation. The protein was purified and labeled as for the wild-type form except that its behaviour on the Q Sepharose column was completely different, probably because of its much higher hydrophobicity. This chromatography step was modified in the following way: the NBD-labeled sample was first applied to a small Q Sepharose column (8 ml). A large fraction of T6 was not retained on this column, so the flow through was then reloaded on a second and larger Q Sepharose column (40 ml). Next, a gradient of NaCl (0–1 M) was applied, which did not elute the T6 mutant but, instead, a few contaminants. Last, the T6 mutant was eluted by repeated injections of 6 M guanidine (3–5 ml). Each injection resulted in the elution of pure NBD-labeled T6 α-synuclein. The various guanidine fractions were then pooled, dialyzed against buffer (50 mM Hepes, pH 7.2, and 120 mM K acetate) and concentrated using a filtration system (cutoff of 3 kD; Amicon Ultra-15; Millipore).

**Liposome preparation and binding assay**

A lipid film containing the desired amount of phospholipids and cholesterol was prepared in a rotary evaporator from stock solutions in chloroform (Avanti Polar Lipids, Inc.). The film was resuspended in 50 mM Hepes, pH 7.2, and 120 mM K acetate at a final concentration of 2 mM phospholipids. After five steps of freezing and thawing using liquid nitrogen and a water bath at 30°C, the liposomes were sequentially extruded using a hand extruder (Avanti Polar Lipids, Inc.) through polycarbonate filters with a pore size of 200, 100, 50, and 30 nm. Alternatively, the liposomes were sonicated with a titanium probe. The size distribution of all liposome suspensions was determined by dynamic light scattering using a Dynapro apparatus at a final concentration of 0.2 mM phospholipids. NBD fluorescence emission was recorded at 37°C upon excitation at 505 nm in a fluorimeter (RF5301; Shimadzu). All experiments were performed in the following buffer: 50 mM Hepes, pH 7.2, 120 mM K acetate, 1 mM $MgCl_2$, and 1 mM DTT. The partition coefficients of [NBD]$GMAP_N$ and [NBD]α-synuclein for liposomes of defined size and composition were determined from two independent titration experiments (Figs. 2 C and 3 B, insets). The partition coefficient corresponds to the amount of free phospholipid that gives 50% binding. For weak binding, this corresponds to the total phospholipid concentration at which the NBD fluorescence change is 50% of maximal. For strong binding, the binding curves were fitted to a quadratic equation describing the binding of a protein to a lipid patch of *n* lipids with an equilibrium constant *K*. The partition coefficient is given by the product *nK* (Mesmin et al., 2007).

**Fluorescence microscopy**

Cultures were grown to mid–logarithmic phase in the appropriate medium at 23°C and then resuspended in fresh synthetic medium and transferred to slide chambers (ibidi; Biovalley) precoated with concanavalin A (Sigma-Aldrich). Cells were maintained at room temperature and imaged using an HCX Plan Apochromat CS 100×, NA 1.40 objective lens on a microscope (DM IRE2; Leica) equipped with a 10-MHz charge-coupled device camera ($CoolSNAP_{HQ}$; Roper Scientific) using Metamorph (version 7.6.4.0; Molecular Devices). Deconvolution of z series was performed and analyzed using Metamorph. For quantifications, images were acquired for each condition in at least three independent experiments. In yeast cells, between 50 and 200 puncta (unless otherwise indicated) of GFP- or mCherry-tagged $GMAP_N$, α-synuclein, or chimeras were scored for the presence or absence of the co-expressed marker or dye, and the percentage of puncta with the coexpressed marker was calculated. All experiments show means and SDs of at least three independent experiments. Preliminary experiments and the experiment shown in Fig. S4 E were performed with the help of the IMAGIF facility in confocal microscopy and flow cytometry, Centre de Recherche de Gif.

**EM**

For ultrastructural experiments, cells were fixed directly in culture medium by addition of 25% glutaraldehyde (Sigma-Aldrich) to a final concentration of 0.5% for ≥10 min with shaking. Cells were harvested, washed twice, and resuspended in 2% glutaraldehyde, 0.1 M cacodylate, pH 6.8, and 1 M sorbitol buffer and incubated overnight or longer at 4°C. Cells were permeabilized in 1% sodium metaperiodate for 15 min at room temperature and then postfixed for 1.5 h at room temperature in a 1:1 mixture of 2% aqueous osmium tetroxide and 3% aqueous potassium ferrocyanide. Cells were embedded in 2% agar and dehydrated in graded ethanol baths (70–100%) followed by embedding in Epon. 70-nm sections were cut with a ultramicrotome (Ultracut UCT; Leica) and counterstained with lead citrate for 1.5 min before observation.

For immunogold labeling, cells were fixed in culture medium (see previous paragraph), washed twice, resuspended in 1% glutaraldehyde cacodylate buffer, and incubated at room temperature for 1 h. Cells were washed and resuspended in 0.1 M cacodylate, pH 6.8, and 1 M sorbitol buffer. Cells were permeabilized in metaperiodate (see previous paragraph) and then incubated for 10 min in 50 mM ammonium chloride and washed in water before embedding in 2% agar. Dehydration was performed in graded ethanol baths (50–100%) followed by embedding in unicryl resin. 90-nm-thick sections were blocked in buffer T (20 mm Tris-HCl, 154 mM NaCl, 0.1% $NaN_3$, 0.1% BSA, 0.05% Tween 20, and 0.1% fish gelatin), incubated with primary GFP antibody (ab290; 1:100; Abcam) in buffer T for 90 min, washed, labeled with 10-nm gold-conjugated anti–rabbit secondary antibodies (Sigma-Aldrich), and stained in 5% uranyl acetate for 5 min followed by lead citrate for 1.5 min. Images in Figs. 1, 5, and S1 were captured on an electron microscope (CM12; FEI) equipped with a 2,048 × 2,048–pixel camera (UltraScan1000; Gatan, Inc.) and DigitalMicrograph acquisition software (Gatan, Inc.). Images in the remaining figures were obtained using a microscope (Morgagni; FEI) fitted with a camera (Morada; Olympus) with Soft Imaging Solutions imaging software (Olympus). Images were tiled with IMOD Blendmont software (Kremer et al., 1996) and then subjected to γ and contrast adjustment.

**Cell staining, CPY secretion, and immunoprecipitation assays**

For FM4-64 staining (Vida and Emr, 1995), cells were incubated with 20 µg/ml FM4-64 (Invitrogen) in YPD medium on ice for 45 min, washed, and incubated at 23°C with shaking for 45 min. To quantify the amount of FM4-64 accumulated in the vacuolar membranes of cells, images of 10 cells per strain were analyzed for each experiment. Using ImageJ software (National Institutes of Health), the mean gray value was determined for vacuolar membrane regions and for regions of the cytoplasm, and the values for vacuolar membranes were normalized against cytoplasmic background levels. Values shown are means and SDs of at least three independent experiments. For Lucifer yellow and Hoechst staining, BY4742 cells carrying the appropriate plasmid were grown overnight ($OD_{600}$ ≈0.1 for Lucifer yellow staining) in selective medium without doxycycline. Cells were spun down and resuspended in YPD containing 4 mg/ml Lucifer yellow (Sigma-Aldrich) or in 1 ml Hoechst dye (0.5 µg/ml) in fresh selective medium and incubated at 23°C for 2.5 h. After washing out the dye, cells were observed in ibidi slide chambers.

To monitor CPY secretion, strains IPY4, IPY5, and IPY6 were grown overnight at 23°C in YP medium containing 2% galactose. Cells were lysed with glass beads (Sigma-Aldrich) in 20 mM Hepes, pH 7.2, 100 mM KCl, 5 mM $MgCl_2$, 1% Nonidet P-40 containing protease inhibitors (GE Healthcare), and PMSF (Sigma-Aldrich), and cleared lysates were resolved

by SDS-PAGE. Immunoblotting with CPY antibody was followed by chemiluminescent detection using ECL Advance Western Blotting Detection kit (GE Healthcare). Membranes were imaged using a luminescent image analyzer (LAS-3000; Fujifilm). The levels of the CPY p1 precursor and mature form were quantified using ImageJ software. The amount of p1 CPY was normalized to total (P1 + mature) CPY. Means and SDs of at least three independent experiments were determined.

The $GMAP_N$ protein/phospholipid ratio in yeast cells was calculated as follows. The quantity of $GMAP_N$-GFP in cell extracts was quantified from Western blots as described in the previous paragraph using ImageJ software and determined to be 35.6 ng (0.5 pmol) per $10^6$ cells (Fig. S1). This quantity corresponds to a concentration of ~7.1 µM, assuming a volume of 70 $µm^3$ for a *Saccharomyces cerevisiae* cell (Sherman, 2002). For comparison, the total concentration of cytoplasmic actin is 5.3 µM (Kim et al., 2004). The total quantity of phospholipids in *S. cerevisiae* has been determined to be 1.03 nmol per $10^6$ cells (Ejsing et al., 2009) or 15 mM. A conservative estimate is that at least half of yeast phospholipids are in bilayers exposed to the cytoplasm, based on calculations of the surface area of yeast organelles and the fact that the majority of phospholipids are in bilayer membranes (Stace and Ktistakis, 2006; Perktold et al., 2007; Bankaitis et al., 2010). Hence, the ratio of $GMAP_N$-GFP protein/phospholipid in bilayers available to bind cytoplasmic $GMAP_N$-GFP is ~1:1,000.

Immunoprecipitations were performed as previously described (Deng et al., 2009), except that the lysis buffer used was 20 mM Hepes, pH 7.2, 100 mM KCl, 5 mM $MgCl_2$, and 1% Nonidet P-40. Cleared cell lysates were incubated for 1 h at 4°C with GFP or α-synuclein antibodies and then with protein G–Sepharose (GE Healthcare) for an additional 1 h at 4°C. The resin was washed three times with 20 mM Hepes, pH 7.2, 100 mM KCl, 5 mM $MgCl_2$, and 0.5% Nonidet P-40 and once with PBS.

**Online supplemental material**

Fig. S1 shows fluorescence and immuno-EM characterization of yeast cells expressing $GMAP_N$-GFP and comparison with cells expressing α-synuclein–GFP. Fig. S2 shows that α-synuclein, but not $GMAP_N$, requires PS for binding to liposomes in vitro. Fig. S3 shows binding of the T6 α-synuclein mutant to large neutral liposomes and expression of T6 α-synuclein in yeast cells. Fig. S4 shows that $GMAP_N$, α-synuclein, and the α-synuclein chimera structures do not colocalize with coats in yeast cells. Fig. S5 compares α-synuclein and the α-synuclein chimera localizations and interactions in wild-type yeast, and their inhibition in the endocytosis mutant *sla2Δ*. Table S1 shows yeast strains used in this study. Online supplemental material is available at http://www.jcb.org/cgi/content/full/jcb.201011118/DC1.

We thank Magali Prigent and Marie-Hélène Cuif for confocal microscopy expertise, Jean Daraspe for EM assistance, Romain Gautier for molecular models, Mélanie Brémond and Lilas Radjou for constructions, and Alain Rambourg for stimulating discussions.

This work was funded by grants from the Agence Nationale de la Recherche, the Fondation pour la Recherche Médicale, and by the Centre National de la Recherche Scientifique. V. Morello was supported by a Ministère de l'Enseignement Supérieur et de la Recherche fellowship.

Submitted: 22 November 2010
Accepted: 16 June 2011

## References

Antonny, B. 2011. Mechanisms of membrane curvature sensing. *Annu. Rev. Biochem.* 80:101–123. doi:10.1146/annurev-biochem-052809-155121

Auluck, P.K., G. Caraveo, and S. Lindquist. 2010. α-Synuclein: membrane interactions and toxicity in Parkinson's disease. *Annu. Rev. Cell Dev. Biol.* 26:211–233. doi:10.1146/annurev.cellbio.042308.113313

Bankaitis, V.A., C.J. Mousley, and G. Schaaf. 2010. The Sec14 superfamily and mechanisms for crosstalk between lipid metabolism and lipid signaling. *Trends Biochem. Sci.* 35:150–160. doi:10.1016/j.tibs.2009.10.008

Bellí, G., E. Garí, L. Piedrafita, M. Aldea, and E. Herrero. 1998. An activator/repressor dual system allows tight tetracycline-regulated gene expression in budding yeast. *Nucleic Acids Res.* 26:942–947. doi:10.1093/nar/26.4.942

Ben Gedalya, T., V. Loeb, E. Israeli, Y. Altschuler, D.J. Selkoe, and R. Sharon. 2009. Alpha-synuclein and polyunsaturated fatty acids promote clathrin-mediated endocytosis and synaptic vesicle recycling. *Traffic*. 10:218–234. doi:10.1111/j.1600-0854.2008.00853.x

Bigay, J., J.F. Casella, G. Drin, B. Mesmin, and B. Antonny. 2005. ArfGAP1 responds to membrane curvature through the folding of a lipid packing sensor motif. *EMBO J.* 24:2244–2253. doi:10.1038/sj.emboj.7600714

Bonifacino, J.S., and B.S. Glick. 2004. The mechanisms of vesicle budding and fusion. *Cell*. 116:153–166. doi:10.1016/S0092-8674(03)01079-1

Burré, J., M. Sharma, T. Tsetsenis, V. Buchman, M.R. Etherton, and T.C. Südhof. 2010. Alpha-synuclein promotes SNARE-complex assembly in vivo and in vitro. *Science*. 329:1663–1667. doi:10.1126/science.1195227

Burston, H.E., L. Maldonado-Báez, M. Davey, B. Montpetit, C. Schluter, B. Wendland, and E. Conibear. 2009. Regulators of yeast endocytosis identified by systematic quantitative analysis. *J. Cell Biol.* 185:1097–1110. doi:10.1083/jcb.200811116

Cardenas, J., S. Rivero, B. Goud, M. Bornens, and R.M. Rios. 2009. Golgi localisation of GMAP210 requires two distinct cis-membrane binding mechanisms. *BMC Biol.* 7:56. doi:10.1186/1741-7007-7-56

Castillon, G.A., R. Watanabe, M. Taylor, T.M. Schwabe, and H. Riezman. 2009. Concentration of GPI-anchored proteins upon ER exit in yeast. *Traffic*. 10:186–200. doi:10.1111/j.1600-0854.2008.00857.x

Cormack, B.P., G. Bertram, M. Egerton, N.A. Gow, S. Falkow, and A.J. Brown. 1997. Yeast-enhanced green fluorescent protein (yEGFP) a reporter of gene expression in *Candida albicans*. *Microbiology*. 143:303–311. doi:10.1099/00221287-143-2-303

Cornell, R.B., and S.G. Taneva. 2006. Amphipathic helices as mediators of the membrane interaction of amphitropic proteins, and as modulators of bilayer physical properties. *Curr. Protein Pept. Sci.* 7:539–552. doi:10.2174/138920306779025675

Davidson, W.S., A. Jonas, D.F. Clayton, and J.M. George. 1998. Stabilization of alpha-synuclein secondary structure upon binding to synthetic membranes. *J. Biol. Chem.* 273:9443–9449. doi:10.1074/jbc.273.16.9443

Deng, Y., M.P. Golinelli-Cohen, E. Smirnova, and C.L. Jackson. 2009. A COPI coat subunit interacts directly with an early-Golgi localized Arf exchange factor. *EMBO Rep.* 10:58–64. doi:10.1038/embor.2008.221

Doucet, C.M., J.A. Talamas, and M.W. Hetzer. 2010. Cell cycle-dependent differences in nuclear pore complex assembly in metazoa. *Cell*. 141:1030–1041. doi:10.1016/j.cell.2010.04.036

Drin, G., and B. Antonny. 2010. Amphipathic helices and membrane curvature. *FEBS Lett.* 584:1840–1847. doi:10.1016/j.febslet.2009.10.022

Drin, G., J.F. Casella, R. Gautier, T. Boehmer, T.U. Schwartz, and B. Antonny. 2007. A general amphipathic alpha-helical motif for sensing membrane curvature. *Nat. Struct. Mol. Biol.* 14:138–146. doi:10.1038/nsmb1194

Drin, G., V. Morello, J.F. Casella, P. Gounon, and B. Antonny. 2008. Asymmetric tethering of flat and curved lipid membranes by a golgin. *Science*. 320:670–673. doi:10.1126/science.1155821

Ejsing, C.S., J.L. Sampaio, V. Surendranath, E. Duchoslav, K. Ekroos, R.W. Klemm, K. Simons, and A. Shevchenko. 2009. Global analysis of the yeast lipidome by quantitative shotgun mass spectrometry. *Proc. Natl. Acad. Sci. USA*. 106:2136–2141. doi:10.1073/pnas.0811700106

Ford, M.G., I.G. Mills, B.J. Peter, Y. Vallis, G.J. Praefcke, P.R. Evans, and H.T. McMahon. 2002. Curvature of clathrin-coated pits driven by epsin. *Nature*. 419:361–366. doi:10.1038/nature01020

Frost, A., V.M. Unger, and P. De Camilli. 2009. The BAR domain superfamily: membrane-molding macromolecules. *Cell*. 137:191–196. doi:10.1016/j.cell.2009.04.010

Gitler, A.D., B.J. Bevis, J. Shorter, K.E. Strathearn, S. Hamamichi, L.J. Su, K.A. Caldwell, G.A. Caldwell, J.C. Rochet, J.M. McCaffery, et al. 2008. The Parkinson's disease protein alpha-synuclein disrupts cellular Rab homeostasis. *Proc. Natl. Acad. Sci. USA*. 105:145–150. doi:10.1073/pnas.0710685105

Haering, C.H., J. Löwe, A. Hochwagen, and K. Nasmyth. 2002. Molecular architecture of SMC proteins and the yeast cohesin complex. *Mol. Cell*. 9:773–788. doi:10.1016/S1097-2765(02)00515-4

Hatzakis, N.S., V.K. Bhatia, J. Larsen, K.L. Madsen, P.Y. Bolinger, A.H. Kunding, J. Castillo, U. Gether, P. Hedegård, and D. Stamou. 2009. How curved membranes recruit amphipathic helices and protein anchoring motifs. *Nat. Chem. Biol.* 5:835–841. doi:10.1038/nchembio.213

Jahn, R., and R.H. Scheller. 2006. SNAREs—engines for membrane fusion. *Nat. Rev. Mol. Cell Biol.* 7:631–643. doi:10.1038/nrm2002

Jao, C.C., B.G. Hegde, J. Chen, I.S. Haworth, and R. Langen. 2008. Structure of membrane-bound alpha-synuclein from site-directed spin labeling and computational refinement. *Proc. Natl. Acad. Sci. USA*. 105:19666–19671. doi:10.1073/pnas.0807826105

Johnson, A.E. 2005. Fluorescence approaches for determining protein conformations, interactions and mechanisms at membranes. *Traffic*. 6:1078–1092. doi:10.1111/j.1600-0854.2005.00340.x

Kahle, P.J., M. Neumann, L. Ozmen, V. Muller, H. Jacobsen, A. Schindzielorz, M. Okochi, U. Leimer, H. van Der Putten, A. Probst, et al. 2000. Subcellular localization of wild-type and Parkinson's disease-associated mutant alpha -synuclein in human and transgenic mouse brain. *J. Neurosci.* 20:6365–6373.

Kaksonen, M., Y. Sun, and D.G. Drubin. 2003. A pathway for association of receptors, adaptors, and actin during endocytic internalization. *Cell*. 115:475–487. doi:10.1016/S0092-8674(03)00883-3

Kim, K., A. Yamashita, M.A. Wear, Y. Maéda, and J.A. Cooper. 2004. Capping protein binding to actin in yeast: biochemical mechanism and physiological relevance. *J. Cell Biol.* 164:567–580. doi:10.1083/jcb.200308061

Klemm, R.W., C.S. Ejsing, M.A. Surma, H.J. Kaiser, M.J. Gerl, J.L. Sampaio, Q. de Robillard, C. Ferguson, T.J. Proszynski, A. Shevchenko, and K. Simons. 2009. Segregation of sphingolipids and sterols during formation of secretory vesicles at the trans-Golgi network. *J. Cell Biol.* 185:601–612. doi:10.1083/jcb.200901145

Kremer, J.R., D.N. Mastronarde, and J.R. McIntosh. 1996. Computer visualization of three-dimensional image data using IMOD. *J. Struct. Biol.* 116:71–76. doi:10.1006/jsbi.1996.0013

Larsen, K.E., Y. Schmitz, M.D. Troyer, E. Mosharov, P. Dietrich, A.Z. Quazi, M. Savalle, V. Nemani, F.A. Chaudhry, R.H. Edwards, et al. 2006. Alpha-synuclein overexpression in PC12 and chromaffin cells impairs catecholamine release by interfering with a late step in exocytosis. *J. Neurosci.* 26:11915–11922. doi:10.1523/JNEUROSCI.3821-06.2006

Lee, M.C., E.A. Miller, J. Goldberg, L. Orci, and R. Schekman. 2004. Bi-directional protein transport between the ER and Golgi. *Annu. Rev. Cell Dev. Biol.* 20:87–123. doi:10.1146/annurev.cellbio.20.010403.105307

Liu, J., Y. Sun, G.F. Oster, and D.G. Drubin. 2010. Mechanochemical crosstalk during endocytic vesicle formation. *Curr. Opin. Cell Biol.* 22:36–43. doi:10.1016/j.ceb.2009.11.009

Liu, S., K.A. Wilson, T. Rice-Stitt, A.M. Neiman, and J.A. McNew. 2007. In vitro fusion catalyzed by the sporulation-specific t-SNARE light-chain Spo20p is stimulated by phosphatidic acid. *Traffic*. 8:1630–1643. doi:10.1111/j.1600-0854.2007.00628.x

Longtine, M.S., A. McKenzie III, D.J. Demarini, N.G. Shah, A. Wach, A. Brachat, P. Philippsen, and J.R. Pringle. 1998. Additional modules for versatile and economical PCR-based gene deletion and modification in *Saccharomyces cerevisiae*. *Yeast*. 14:953–961. doi:10.1002/(SICI)1097-0061(199807)14:10<953::AID-YEA293>3.0.CO;2-U

McMahon, H.T., and J.L. Gallop. 2005. Membrane curvature and mechanisms of dynamic cell membrane remodelling. *Nature*. 438:590–596. doi:10.1038/nature04396

Mesmin, B., G. Drin, S. Levi, M. Rawet, D. Cassel, J. Bigay, and B. Antonny. 2007. Two lipid-packing sensor motifs contribute to the sensitivity of ArfGAP1 to membrane curvature. *Biochemistry*. 46:1779–1790. doi:10.1021/bi062288w

Middleton, E.R., and E. Rhoades. 2010. Effects of curvature and composition on α-synuclein binding to lipid vesicles. *Biophys. J.* 99:2279–2288. doi:10.1016/j.bpj.2010.07.056

Nakanishi, H., P. de los Santos, and A.M. Neiman. 2004. Positive and negative regulation of a SNARE protein by control of intracellular localization. *Mol. Biol. Cell*. 15:1802–1815. doi:10.1091/mbc.E03-11-0798

Nemani, V.M., W. Lu, V. Berge, K. Nakamura, B. Onoa, M.K. Lee, F.A. Chaudhry, R.A. Nicoll, and R.H. Edwards. 2010. Increased expression of alpha-synuclein reduces neurotransmitter release by inhibiting synaptic vesicle reclustering after endocytosis. *Neuron*. 65:66–79. doi:10.1016/j.neuron.2009.12.023

Outeiro, T.F., and S. Lindquist. 2003. Yeast cells provide insight into alpha-synuclein biology and pathobiology. *Science*. 302:1772–1775. doi:10.1126/science.1090439

Perktold, A., B. Zechmann, G. Daum, and G. Zellnig. 2007. Organelle association visualized by three-dimensional ultrastructural imaging of the yeast cell. *FEM. Yeast Res.* 7:629–638. doi:10.1111/j.1567-1364.2007.00226.x

Rein, U., U. Andag, R. Duden, H.D. Schmitt, and A. Spang. 2002. ARF-GAP–mediated interaction between the ER-Golgi v-SNAREs and the COPI coat. *J. Cell Biol.* 157:395–404. doi:10.1083/jcb.200112092

Rossi, G., and P. Brennwald. 2011. Yeast homologues of lethal giant larvae and type V myosin cooperate in the regulation of Rab-dependent vesicle clustering and polarized exocytosis. *Mol. Biol. Cell*. 22:842–857. doi:10.1091/mbc.E10-07-0570

Roy, M.O., R. Leventis, and J.R. Silvius. 2000. Mutational and biochemical analysis of plasma membrane targeting mediated by the farnesylated, polybasic carboxy terminus of K-ras4B. *Biochemistry*. 39:8298–8307. doi:10.1021/bi000512q

Sato, K., and A. Nakano. 2003. Oligomerization of a cargo receptor directs protein sorting into COPII-coated transport vesicles. *Mol. Biol. Cell*. 14:3055–3063. doi:10.1091/mbc.E03-02-0115

Schneiter, R., B. Brügger, R. Sandhoff, G. Zellnig, A. Leber, M. Lampl, K. Athenstaedt, C. Hrastnik, S. Eder, G. Daum, et al. 1999. Electrospray ionization tandem mass spectrometry (ESI-MS/MS) analysis of the lipid molecular species composition of yeast subcellular membranes reveals acyl chain-based sorting/remodeling of distinct molecular species en route to the plasma membrane. *J. Cell Biol.* 146:741–754. doi:10.1083/jcb.146.4.741

Sclafani, A., S. Chen, F. Rivera-Molina, K. Reinisch, P. Novick, and S. Ferro-Novick. 2010. Establishing a role for the GTPase Ypt1p at the late Golgi. *Traffic*. 11:520–532. doi:10.1111/j.1600-0854.2010.01031.x

Sharpe, H.J., T.J. Stevens, and S. Munro. 2010. A comprehensive comparison of transmembrane domains reveals organelle-specific properties. *Cell*. 142:158–169. doi:10.1016/j.cell.2010.05.037

Sherman, F. 2002. Getting started with yeast. *Methods Enzymol.* 350:3–41. doi:10.1016/S0076-6879(02)50954-X

Soper, J.H., S. Roy, A. Stieber, E. Lee, R.B. Wilson, J.Q. Trojanowski, C.G. Burd, and V.M. Lee. 2008. Alpha-synuclein-induced aggregation of cytoplasmic vesicles in *Saccharomyces cerevisiae*. *Mol. Biol. Cell*. 19:1093–1103. doi:10.1091/mbc.E07-08-0827

Soper, J.H., V. Kehm, C.G. Burd, V.A. Bankaitis, and V.M. Lee. 2011. Aggregation of α-synuclein in *S. cerevisiae* is associated with defects in endosomal trafficking and phospholipid biosynthesis. *J. Mol. Neurosci.* 43:391–405. doi:10.1007/s12031-010-9455-5

Stace, C.L., and N.T. Ktistakis. 2006. Phosphatidic acid- and phosphatidylserine-binding proteins. *Biochim. Biophys. Acta*. 1761:913–926.

Südhof, T.C., and J.E. Rothman. 2009. Membrane fusion: grappling with SNARE and SM proteins. *Science*. 323:474–477. doi:10.1126/science.1161748

Sun, Y., S. Carroll, M. Kaksonen, J.Y. Toshima, and D.G. Drubin. 2007. PtdIns(4,5)P2 turnover is required for multiple stages during clathrin- and actin-dependent endocytic internalization. *J. Cell Biol.* 177:355–367. doi:10.1083/jcb.200611011

Thayanidhi, N., J.R. Helm, D.C. Nycz, M. Bentley, Y. Liang, and J.C. Hay. 2010. Alpha-synuclein delays endoplasmic reticulum (ER)-to-Golgi transport in mammalian cells by antagonizing ER/Golgi SNAREs. *Mol. Biol. Cell*. 21:1850–1863. doi:10.1091/mbc.E09-09-0801

van Meer, G., D.R. Voelker, and G.W. Feigenson. 2008. Membrane lipids: where they are and how they behave. *Nat. Rev. Mol. Cell Biol.* 9:112–124. doi:10.1038/nrm2330

Vida, T.A., and S.D. Emr. 1995. A new vital stain for visualizing vacuolar membrane dynamics and endocytosis in yeast. *J. Cell Biol.* 128:779–792. doi:10.1083/jcb.128.5.779

Voeltz, G.K., W.A. Prinz, Y. Shibata, J.M. Rist, and T.A. Rapoport. 2006. A class of membrane proteins shaping the tubular endoplasmic reticulum. *Cell*. 124:573–586. doi:10.1016/j.cell.2005.11.047

Wickner, W., and R. Schekman. 2008. Membrane fusion. *Nat. Struct. Mol. Biol.* 15:658–664. doi:10.1038/nsmb.1451

Wooding, S., and H.R. Pelham. 1998. The dynamics of golgi protein traffic visualized in living yeast cells. *Mol. Biol. Cell*. 9:2667–2680.

Yeung, T., G.E. Gilbert, J. Shi, J. Silvius, A. Kapus, and S. Grinstein. 2008. Membrane phosphatidylserine regulates surface charge and protein localization. *Science*. 319:210–213. doi:10.1126/science.1152066

Zinser, E., C.D. Sperka-Gottlieb, E.V. Fasch, S.D. Kohlwein, F. Paltauf, and G. Daum. 1991. Phospholipid synthesis and lipid composition of subcellular membranes in the unicellular eukaryote *Saccharomyces cerevisiae*. *J. Bacteriol.* 173:2026–2034.